SANDIA REPORT
SAND 2009-0399
Unlimited Release
Printed January 2009

Summary Report: Direct Approaches for Recycling Carbon Dioxide into Synthetic Fuel

James E. Miller, Lindsey R. Evans, Nathan P. Siegel, Richard B. Diver, Fred Gelbard, Andrea Ambrosini, and Mark D. Allendorf

Prepared by
Sandia National Laboratories
Albuquerque, New Mexico 87185 and Livermore, California 94550

Sandia is a multiprogram laboratory operated by Sandia Corporation,
a Lockheed Martin Company, for the United States Department of Energy's
National Nuclear Security Administration under Contract DE-AC04-94AL85000.

Issued by Sandia National Laboratories, operated for the United States Department of Energy by Sandia Corporation.

Available to DOE and DOE contractors from
U.S. Department of Energy
Office of Scientific and Technical Information
P.O. Box 62
Oak Ridge, TN 37831

Telephone: (865) 576-8401
Facsimile: (865) 576-5728
E-Mail: reports@adonis.osti.gov
Online ordering: http://www.osti.gov/bridge

Available to the public from
U.S. Department of Commerce
National Technical Information Service
5285 Port Royal Rd.
Springfield, VA 22161

Telephone: (800) 553-6847
Facsimile: (703) 605-6900
E-Mail: orders@ntis.fedworld.gov
Online order: http://www.ntis.gov/help/ordermethods.asp?loc=7-4-0#online

SAND 2009-0399
Unlimited Release
Printed January 2009

Summary Report: Direct Approaches for Recycling Carbon Dioxide into Synthetic Fuel

James E. Miller, Lindsey R. Evans, Nathan P. Siegel, Richard B. Diver, Fred Gelbard, Andrea Ambrosini, * Mark D. Allendorf

Sandia National Laboratories
P.O. Box 5800
Albuquerque, NM 87185

*P.O. Box 969
Livermore, CA 94551-0969

Abstract

The consumption of petroleum by the transportation sector in the United States is roughly equivalent to petroleum imports into the country, which have totaled over 12 million barrels a day every year since 2004. This reliance on foreign oil is a strategic vulnerability for the economy and national security. Further, the effect of unmitigated CO_2 releases on the global climate is a growing concern both here and abroad. Independence from problematic oil producers can be achieved to a great degree through the utilization of non-conventional hydrocarbon resources such as coal, oil-shale and tar-sands. However, tapping into and converting these resources into liquid fuels exacerbates green house gas (GHG) emissions as they are carbon rich, but hydrogen deficient. Revolutionary thinking about energy and fuels must be adopted. We must recognize that hydrocarbon fuels are ideal energy carriers, but not primary energy sources.

The energy stored in a chemical fuel is released for utilization by oxidation. In the case of hydrogen fuel the chemical product is water; in the case of a hydrocarbon fuel, water and carbon dioxide are produced. The hydrogen economy envisions a cycle in which H_2O is re-energized by splitting water into H_2 and O_2, by electrolysis for example. We envision a hydrocarbon analogy in which both carbon dioxide and water are re-energized through the application of a persistent energy source (e.g. solar or nuclear). This is of course essentially what the process of photosynthesis accomplishes, albeit with a relatively low sunlight-to-hydrocarbon efficiency. The goal of this project then was the creation of a direct and efficient process for the solar or nuclear driven thermochemical conversion of CO_2 to CO (and O_2), one of the basic building blocks of synthetic fuels. This process would potentially provide the basis for an alternate hydrocarbon economy that is carbon neutral, provides a pathway to energy independence, and is compatible with much of the existing fuel infrastructure.

Table of Contents

List of Figures

List of Tables

1.0 Introduction

1.1 Motivation

The United States is the world's leading importer of petroleum. Since 2004, imports to the U.S. have totaled over 12 million barrels per day (mbpd), accounting for about 60% of the country's daily consumption of over 20 mbpd [1]. In 2007 the U.S. transportation sector consumed 13.9 mbpd of petroleum while global petroleum production totaled only 81.2 mbpd [2]. Hence, in 2007 the U.S. consumed over 25% of the world's petroleum production, consumed over 17% of the world's production for the purpose of transportation, and imported about 15% of the world's total production. This reliance on petroleum imports represents a significant economic vulnerability, particularly to the vital transportation sector. The costs to economy have been large. A study conducted by ORNL concluded that the cost of oil dependence to the U.S. economy from 1970-2004 totaled $8 trillion* [3]. Furthermore, the increasing price of oil has contributed significantly to the trade deficit in recent years [4], accounting for more than half of the deficit in the first quarter of 2008 [5].

The reliance on petroleum imports has national security implications beyond the threat to the economy. Increasing attention has recently been given to the fact that the recent high price of oil is driving one of the largest transfers of wealth in history at a rate of $700 billion a year [6]. Table 1, showing the world's top petroleum importers and exporters, illustrates that this transfer is predominantly away from Western-style democracies.

Table 1. Top Net Petroleum Importers and Exporters in 2006.

Rank	Importer	mbpd	Exporter	mbpd
1	United States	12.4	Saudi Arabia	8.5
2	Japan	5.1	Russia	6.9
3	China	3.4	United Arab Emirates	2.6
4	Germany	2.5	Norway	2.6
5	South Korea	2.1	Iran	2.5
6	France	1.9	Kuwait	2.3
7	India	1.7	Venezuela	2.1
8	Italy	1.6	Nigeria	2.1
9	Spain	1.6	Algeria	1.8
10	Taiwan	0.9	Mexico	1.6

Data taken from reference [7].

This wealth transfer has helped promote "Petroleum-nationalism" in Latin America and elsewhere, and some are as blunt to say that the U.S. and others are funding both sides of the "war on terror" [8]. In any case, it is clear that U.S. dependence on foreign petroleum has significant and likely increasing foreign policy implications. A recent task force report from the Council on Foreign Relations expressed it as follows [9].

> *The lack of sustained attention to energy issues is undercutting U.S. foreign policy and U.S. national security. Major energy suppliers—from Russia to*

* 2005 dollar basis.

> *Iran to Venezuela—have been increasingly able and willing to use their energy resources to pursue their strategic and political objectives. Major energy consumers—notably the United States, but other countries as well—are finding that their growing dependence on imported energy increases their strategic vulnerability and constrains their ability to pursue a broad range of foreign policy and national security objectives. Dependence also puts the United States into increasing competition with other importing countries, notably with today's rapidly growing emerging economies of China and India. At best, these trends will challenge U.S. foreign policy; at worst, they will seriously strain relations between the United States and these countries.*

The reliance on foreign oil is thus a strategic vulnerability for the economy and national security. Independence from problematic oil producers could be achieved to a great degree through the utilization of non-conventional hydrocarbon resources such as coal, oil-shale and tar-sands. This approach has the advantages of consistency with the current fuel infrastructure and a sound and relatively mature technological basis. However, tapping into and converting these resources into liquid fuels exacerbates the problem of green house gas (GHG) emissions as they are carbon rich, but hydrogen deficient. The effect of unmitigated CO_2 releases on the global climate is a growing concern both here and abroad. Accounting for growth as well as improvements in energy efficiency, it is calculated that more than 10 terraWatts of carbon-free power will be required by 2050 just to stabilize global CO_2 levels at 550 ppm [10]. This will of course require massive investment. However, massive investment will also be required to continue the current fossil energy paradigm [11].

Revolutionary thinking is required if the coupled problems of energy (transportation) security and climate change are to both be addressed. Hydrocarbon fuels are ideal energy carriers, but they can no longer be thought of as primary energy sources. Rather, it is necessary that we take the realistic view that our conventional hydrocarbon fuels are in fact "stored sunlight" and "sequestered carbon." That is, petroleum, coal and other fossil fuels are the end result of a long process that begin with a biological organism capturing sunlight and storing the energy of that captured sunlight by using it to drive chemical conversions of CO_2 and H_2O to hydrocarbons and oxygen (photosynthesis). A fraction of these hydrocarbons were then converted over time by heat and pressure to coal and oil. The overall efficiency of these processes in terms of sunlight to fuel was quite low, particularly for oil and natural gas. For oil, the sunlight to stored energy efficiency is estimated to be only about 0.0002%. It follows that the average U.S. gallon of gasoline is estimated to have begun as approximately 90 metric tons of ancient plant matter [12]. Although the efficiency was low, the very long time scales resulted in an accumulation of vast quantities of carbon-based fossil fuels.

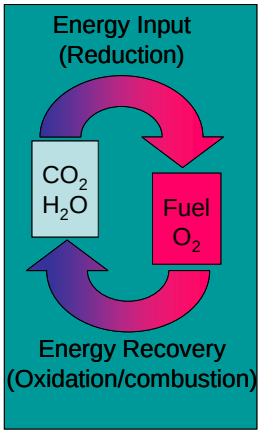

Biofuels, e.g. bio-ethanol, can be thought of as modern approach to improving upon this efficiency, shortening the time scale, and making the process more inherently cyclic and sustainable. As before, the starting point is the photosynthetic conversion of CO_2 and H_2O to hydrocarbons. Additional chemical or biological steps are then undertaken to produce a hydrocarbon fuel. The overall sunlight to fuel efficiency is dependent on location and the process specifics and is thus difficult to define precisely or to generalize. However, it is still generally quite low, although significantly better than that for oil. One can put an upper limit on the biomass approach by considering the efficiency of the photosynthetic step alone. Photosynthesis is generally measured to be 2.5% efficient at best [12], but is currently less than 0.5% for rapidly growing large area crops [10]. It is commonly accepted that the solar to ethanol efficiency from corn kernels is less than 1% [13]. The maximum possible efficiency is estimated to be 4.6% for C3 photosynthesis and 6% for C4 photosynthesis, under current atmospheric conditions [14].

Figure 1 provides some perspective on the importance of using sunlight efficiently. This figure shows the approximate land area required to produce 20 mbpd of oil equivalent (energy basis, assuming 6120 MJ/barrel) assuming a given sunlight-to-fuel efficiency across the totality of the area, and the generous assumption of uniform irradiance across the area at an average rate of that realized in Albuquerque, NM (2600 kWh/m^2/yr). As shown in the figure, at this rate, an area the size of Delaware receives an amount of sunlight equivalent in energy content to our daily petroleum consumption. If sunlight could be converted to a petroleum equivalent at an overall efficiency of 10%, the area increases to only the size of New Jersey and Massachusetts combined. At 3% efficiency the required area increases to the size of Georgia. However, at 0.1%, a level commensurate with many biofuels options, an area equivalent to the entire western half of the U.S. is required. It is thus clear that the efficiency of any proposed solar to fuel conversion process is a fundamental consideration.

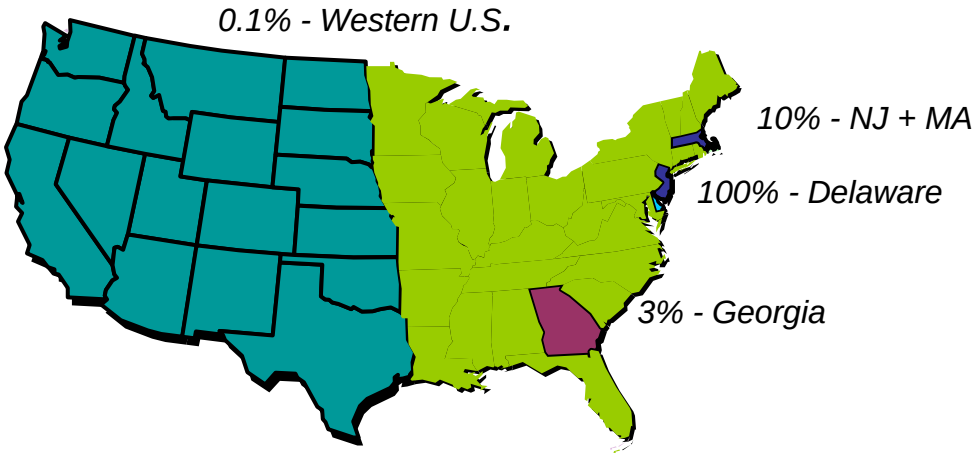

Figure 1. Nominal land areas required to produce 20 mbpd oil equivalents at given sunlight-to-fuel efficiencies assuming uniform solar resource of 2600 kWh/m^2/yr.

As a final consideration, there are of course other options for chemical CO_2 utilization and/or minimization other than conversion to hydrocarbon fuels. Conventional thought along these lines is illustrated by a recent National Academies report [15] and a book summarizing a recent EU project [16]. In these and similar reports, much attention is

given to topics such as sequestration, biomass energy, increased energy and feedstock utilization efficiency, and supercritical CO_2 as a solvent or reaction media. Further, the conversion chemistry that is often most fully considered is that of using CO_2 as a "green" intermediate for introducing specific functionalities into organic compounds. Although this chemistry is sometimes very elegant, the relatively small volumes that would be used render these approaches almost irrelevant from a greenhouse gas point of view [17].

Table 2 illustrates this point. The polymer precursors ethylene, propylene, and ethylene dichloride are three largest commodity chemicals produced in the United States. The third column of the table shows the amount of CO_2 that could be consumed annually as a feedstock to produce these chemicals assuming 100% carbon efficiency in a CO_2 utilization scheme. For example, the carbon in one mole of ethylene (C_2H_4) or ethylene dichloride ($C_2H_4Cl_2$) could theoretically be provided by 2 moles of CO_2; thus one pound of ethylene could theoretically consume 3.14 pounds of carbon dioxide. The 2004 emissions of CO_2 in the United States tied to fossil energy sources are provided in the bottom rows. A comparison shows that a CO_2 utilization scheme for chemical production, although potentially valuable, would account for only a small fraction of the CO_2 being produced. The CO_2 equivalents of the three leading chemicals amount to only 5.7% of the CO_2 resulting from combustion of petroleum products and only 2.4% of that tied to petroleum, coal and natural gas. The only potential product family that could consume CO_2 feedstock at a level commensurate with current emissions is hydrocarbon fuels.

Table 2. Potential Impact of Using CO_2 as a Feedstock for Chemical Production.

	2004 U.S. production [18] (1,000 metric tons)	CO_2 equivalents (1,000 metric tons)
Ethylene	25,682	80,641
Propylene	15,345	48,183
Ethylene dichloride	12,163	10,811
Sum of Top 3 U.S. Chemicals		139,635
U.S. Petroleum [19]		2,458,000
Petroleum, Coal, NG [19]		5,705,000

1.2 Project Goal and Outline

The broad goal of this project was to develop technology for efficiently converting CO_2 and H_2O, the same basic building blocks nature uses, to hydrocarbon fuels, using only sustainable, carbon-neutral energy sources. Specifically the project focused on the creation of a direct and efficient CO_2 splitting ($2CO_2 \rightarrow 2CO + O_2$) process that can be efficiently driven by nuclear or solar sources of thermal energy. Part of our rationale for

CO_2 splitting (CDS) being a foundation for synfuel production has been outlined in an earlier report arising from this project [20].

Briefly, CO is one fundamental component, the other being H_2, of syngas, the key intermediate for synfuel production. Reactions of syngas to form hydrocarbons are thermodynamically downhill. Hydrogen can be produced renewably with commercially available technologies, e.g. via photovoltaic-driven electrolysis. A reasonable starting estimate for the solar-to-hydrogen efficiency is about 9% (0.12(PV) x 0.75(electrolysis) = 0.09). Hydrogen may then be reacted with CO_2 to directly produce methanol, or indirectly to produce CO and then methanol, for example. The reactions of CO_2 and H_2 are generally not very thermodynamically favorable (defined here as having a negative Gibbs free energy of reaction). (For example, the reverse water gas shift reaction is favorable only at very high temperatures and the direct synthesis of methanol is favorable only at temperatures lower than those required to carry out the conversion.) Nonetheless, it has been calculated that current technology would allow hydrocarbons to be manufactured from CO_2 and electrolytic H_2 with an electrical to hydrocarbon efficiency of roughly 40-50% [21]. Thus a 5% sunlight-to-fuel efficiency is plausible for a PV-driven fuel production process.

Thermochemical cycles for water splitting are under development in our laboratories [22,23] and elsewhere [24]. These avoid the efficiency-sapping sunlight to electrical energy conversion required for electrolysis and may somewhat improve the overall efficiency of both hydrogen and subsequent hydrocarbon production. Additionally, at high temperatures, CO_2 is thermodynamically less stable than H_2O. Thus, thermochemically splitting CO_2 in a process analogous to water splitting is thermodynamically feasible and also provides a direct route to manufacture CO for syngas and hydrocarbon production.

Cycles for splitting CO_2 (or H_2O) are endothermic and generally require at least one high temperature step to drive the reaction. Concentrating solar power (CSP) and nuclear energy (NE) can efficiently supply heat in excess of 800 °C and are ideally suited to thermochemical cycles. Thermochemical cycles are typically categorized by temperature range. High temperature (HT) cycles are those that operate within the limits of most engineering materials and typically involve temperatures between 600 and 1000 °C. Ultra-high temperature (UHT) cycles require heat input at temperatures in excess of 1000 and up to 3000 °C. Only CSP can be applied to these cycles as materials constraints preclude NE above about 900 °C. The intention of this project was to address both temperature regimes

For the first year the project had three basic thrusts. The goal of the first thrust was to identify and demonstrate a UHT metal oxide-based system for CDS in the laboratory. Ferrite and ceria-based systems were considered strong initial candidates. Success in the laboratory was to be followed by demonstration of the chemistry on-sun at the National Solar Thermal Test Facility (NSTTF.) The goal of the second thrust was identifying and demonstrating an HT cycle or cycles that is compatible with both next-generation nuclear energy and concentrating solar power (maximum temperatures < 900 ºC). The goal of

the third thrust was to support the first two thrusts by developing an automated tool linked to a thermodynamic database that search for new CDS cycles, thereby allowing us to go beyond our own chemical intuition.

During the second year, the project focused more narrowly on the UHT solar-driven metal oxide thermochemical cycle and provided the basis for new and larger efforts currently termed "Sunshine to Petrol."

2.0 Ultra High Temperature Metal Oxide Cycles for Splitting CO_2

2.1 Introduction and Review of Candidate Materials

Thermochemical cycles have conventionally been studied as potentially a more straightforward, efficient, and lower cost approach to hydrogen production than using electric power to electrolyze water. In the water splitting (WS) scenario, thermochemical cycles employ reactive materials or fluids in a series of chemical reactions that sum to the overall water splitting reaction

$$H_2O \rightarrow H_2 + ½\ O_2.$$

One class of thermochemical cycles utilizes metal oxides as the internally recycled working material. Fe_3O_4 is the prototypical working material for these cycles. The overall idealized reaction scheme is:

$$Fe_3O_4 \rightarrow 3\ FeO + ½\ O_2$$
$$3\ FeO + H_2O \rightarrow Fe_3O_4 + H_2$$

In practice, the temperature required to thermally reduce Fe_3O_4 to any significant extent is in excess of the melting point of both the oxide reactant and product, while the temperature of the hydrogen producing step is below the melting points. This inherent phase change renders the process unworkable as written. One strategy that has been developed to overcome this problem is to substitute other metals into the Fe_3O_4 framework that have the effect of lowering the reduction temperature while maintaining the overall spinel structure. Not including the possibility of solution formation, an overall idealized reaction scheme for these modified materials is:

$$A_xFe_{3-x}O_4 \rightarrow xAO + (3-x)FeO + 0.5\ O_2$$
$$xAO + (3-x)FeO + H_2O \rightarrow A_xFe_{3-x}O_4 + H_2$$
$$\text{Where } 0 \leq x \leq 1$$

Among the A metals considered are Mn, Co, Ni, and Zn. It has also been demonstrated that further advantage is obtained by supporting the mixed oxides on zirconia or yttria-stabilized zirconia (YSZ) as this tends to limit sintering and prevent deactivation after several cycles. For a review of thermochemical WS see [24], and for a discussion of the thermodynamics of substituted ferrites, including solution formation, refer to [23].

2.1.1 Ferrites

In this project, the CDS reaction was considered to be analogous to the WS reaction. Thus it was postulated that mixed metal ferrites of the type $A_xFe_{3-x}O_4$, with $0 \leq x \leq 1$, and A chosen as one or more of the following: Mn, Co, Ni, Zn, Mg, Cu (possibly others) should split CO_2 according to the following idealized scheme:

$$A_xFe_{3-x}O_4 \rightarrow xAO + (3-x)FeO + 0.5\ O_2 \text{ (Thermal Reduction)}$$
$$xAO + (3-x)FeO + CO_2 \rightarrow A_xFe_{3-x}O_4 + CO \text{ (CO Generation)}$$

The scheme is considered idealized because the thermal reduction does not need to proceed to completion in order for the scheme to be workable. That is, it is not necessary for the FeO and AO phases to form; an oxygen deficient spinel or other phase should suffice. Further, it is not necessary or probably desirable for the A and Fe phases to split as suggested by idealized CO generation reaction. That is, AO and FeO could also be present as a single solution or multiple mixed phases. With these considerations in mind, a more general scheme is:

$$F \rightarrow ODF + \tfrac{1}{2}yO_2$$

$$ODF + yCO_2 \rightarrow F + yCO$$

Where F = Ferrite ($A_xFe_{3-x}O_4$, $0 \leq x \leq 1$)

ODF = Oxygen Deficient Ferrite or Ferrites ($A_xFe_{3-x}O_{4-y}$, $0 \leq x \leq 1$, and $0 < y \leq 1$).

Additionally, based on results with WS, it was assumed that the use of zirconia or YSZ supports for the ferrites would offer some advantage.

One concern with the ferrite approach is the possibility that carbon deposits could form on the ferrites or alternately that carbides could form either of which would limit the utility of the ferrite family for this application. Certainly carbon formation is a concern in steam and dry reforming (reaction of CO_2 and CH_4) over Fe- and Ni-containing catalysts, and Ni and Fe are known to catalyze the growth of carbon fibers or filaments. Carbide formation via reaction of iron oxide with syngas or CO is a key step in activating Fischer Tropsch catalysts [25]. The thermodynamics of several possible detrimental reactions are shown in Figure 2 and Figure 3. These figures verify that many of these reactions are indeed favorable at temperatures that could be encountered in a working thermochemical system.

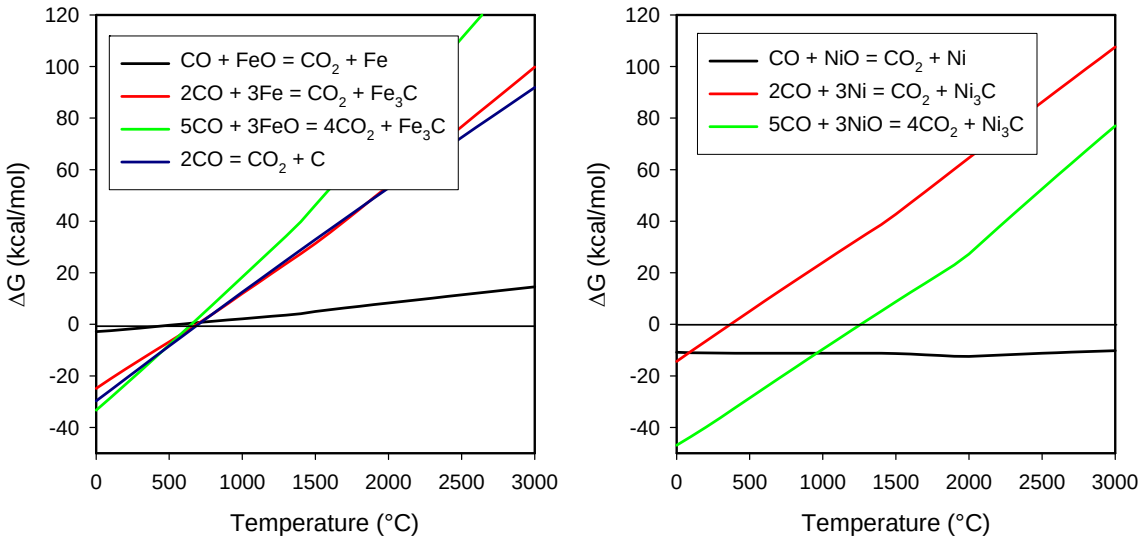

Figure 2. Thermodynamic calculations for potentially problematic reactions of CO including carbon deposition (coke formation) via the Boudouard reaction, reduction of iron and nickel oxide, and iron and nickel carbide formation. Calculations performed for reactions as written using HSC chemistry for Windows 5.1.

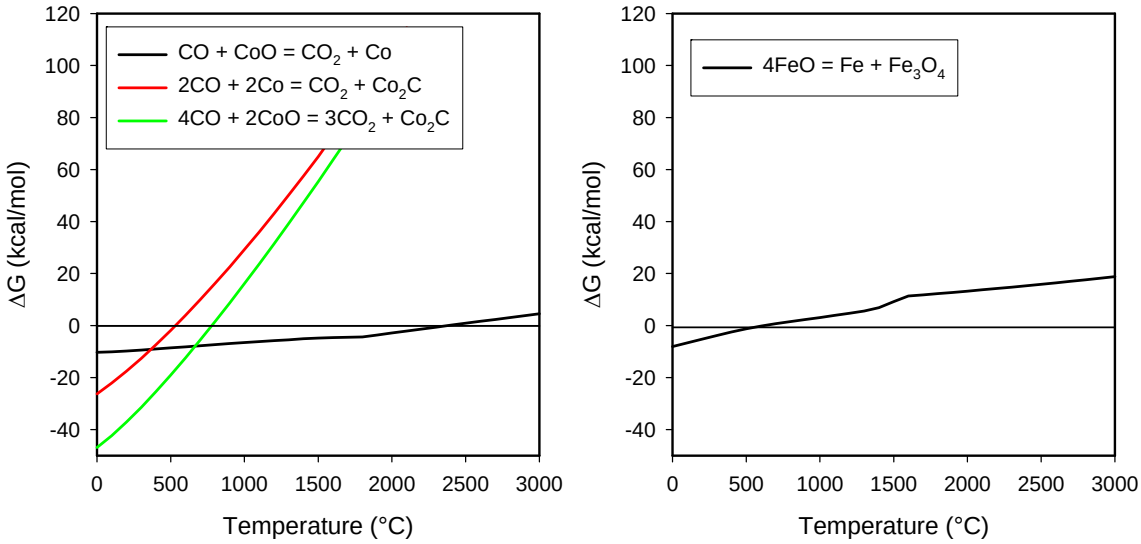

Figure 3. Thermodynamic calculations for potentially problematic reactions of CO including reduction of cobalt oxide, cobalt carbide formation, and the disproportionation of wustite (FeO). Calculations performed for reactions as written using HSC chemistry for Windows 5.1.

A review of the literature reveals that carbon deposition on reduced ferrites has been the focus/goal of several research groups. To the best of our knowledge, Tamaura and Tahata [26] were the first to report the use of a partially reduced ferrite to specifically reduce carbon dioxide. In this case CO_2 was reacted over "cation-excess" magnetite ($Fe_{3+\delta}O_4$, δ=0.127; note that this could also be treated as oxygen deficient magnetite: $Fe_3O_{3.84}$) at 290 ºC to yield a zero-valent carbon deposit. In turn, oxygen was transferred to the magnetite, driving it towards the fully oxidized state. It was later shown that Rh could catalyze both the magnetite activation and carbon deposition [27]. Note that in this initial and in the follow-on work by Tamaura and others, the temperature of the CO_2 decomposition reaction was low, and that the ferrite phase was chemically (in this case by reacting with H_2) rather than thermally reduced.

In further work, Tamaura and coworkers demonstrated similar behavior in several other mixed metal ferrites. Increasing amounts of Ni and Co substitution increased the reactivity of H_2-reduced ferrites [28]. Rates for carbon deposition at 300 °C were improved over H_2-activated magnetite by a factor of 30 for a reduced Ni(II)-bearing ferrite, $Ni_{0.37}Fe_{2.58}O_4$ [28,29] As was observed for the magnetite, impregnating the Ni-ferrite with catalytic metals (Rh, Pt, Ce) further increased the rate of CO_2 decomposition and H_2 reduction; Ce did not improve the reduction step [30].

In contrast to results for Ni-substituted materials, the presence of Mn in the spinel greatly decreased the rate of CO_2 decomposition; the rate of decomposition over a H_2-activated spinel with a composition of Fe:Mn ≈ 2:1 was about 10^5 times less than that over the pure magnetite [31,32] This effect was attributed to a reduction in electron conductivity. Reducing the Mn-substituted ferrite all the way to a wustite (Mn-substituted FeO) phase improves the reactivity at 400 °C over the spinel. In a batch system, the reaction was observed to proceed stepwise from CO_2 to CO to C over the mangano-wustite [33]. The

decomposition over a H_2-reduced Zn-ferrite was also found to proceed in two steps: the decomposition of CO_2 to CO followed by the decomposition of adsorbed CO into C [34]. In this case, a phase separation occurred and Zn oxide and wustite phases were formed upon the initial H_2 reduction. The Tamaura group eventually demonstrated methanation of the carbon deposits (reaction of the C with H_2 to form CH_4) formed on several of the ferrite materials [35,36,37]. Ultimately the two steps, reduction and methanation, were put together and demonstrated in a bench-scale system as a method of recycling CO_2 [38].

In related, but more recent work, Kim et al. described the preparation of nano-sized Ni,Zn)-ferrites for decomposing CO_2 [39]. As in the work of the Tamaura group, the ferrites were activated by H_2 reduction. A second group in Korea has investigated the use of reduced Cu-ferrites for decomposing CO_2 [40,41]. There are two interesting twists to this work. First, CO_2 is reduced to CO rather than C over this material. Second, they have demonstrated that the Cu-ferrite material can be reduced with methane rather than H_2. Although higher temperatures are required (700 ºC), methane reduction produces a useful syngas ($CO + 2\ H_2$) product along with the reduced ferrite. Thus a coupled cyclic system could convert natural gas to syngas and convert CO_2 to CO.

Finally, the use of reduced metal powders (Fe, Zn, and Mg) for converting CO_2 bubbled through a pH 4 solution has been considered [42]. CO was produced over Zn, methane was produced over Mg, and methane, ethane and ethylene were produced over Fe. The source of the reduced metals or energy required to produce or recycle them was not explicitly considered.

2.1.2 Ceria and Mixed Metal Cerium Oxides

Thermochemical water splitting cycles based on the CeO_2/Ce_2O_3 pair were very recently reported and demonstrated [43].

$$2\ CeO_2 \rightarrow Ce_2O_3 + ½\ O_2$$
$$Ce_2O_3 + H_2O \rightarrow 2\ CeO_2 + H_2$$

To the best of our knowledge an analogous cycle has not been reported or contemplated for splitting CO_2.

$$2\ CeO_2 \rightarrow Ce_2O_3 + ½\ O_2$$
$$Ce_2O_3 + CO_2 \rightarrow 2\ CeO_2 + CO$$

However, the application of ceria to this process appears to have several potential advantages over ferrites. These include higher melting points for the oxides, potentially lower reduction temperatures for the oxides, and perhaps most importantly, the lack of a tendency to support carbon deposition.

In addition to these advantages, the reaction chemistry seems very favorable. Each of the individual reaction steps is supported by the literature. The ability of ceria to store and release oxygen in response to its environment is well known and this function has found utility in many applications including automotive catalysts, oxidation catalysts, reforming catalysts, and as an anode for solid oxide fuel cells. Probably the most known catalytic application is as an oxygen storage material in three-way automotive catalysts. Ceria readily donates and accepts oxygen as the cerium cation switches oxidation states from

Ce(IV) to Ce(III) and back as vacancies are formed and annihilated (within a limited range of stoichiometry). Of potential importance is the fact that partially reduced ceria is both an ionic and electronic conductor. (The electronic conductivity for *pure* reduced ceria dominates [44].) As already noted, the thermal reduction step to create an active reduced phase was recently demonstrated in the context of a water splitting cycle [43].

In regards to the second reaction of the cycle, Sharma et al. [45] presented direct evidence for the oxidation of reduced ceria by CO_2 and the concomitant production of CO in a paper published in 2000. In this case, a Pd catalyst was present on the ceria surface; it was not stated whether (or at what rate) the reaction proceeded in the absence of the Pd. In a similar report, Bernal et al. reported that CO_2 could be used to reoxidize Pt-loaded ceria at 200 ºC. In this case, the resulting CO was chemisorbed on the Pt [46]. Additional reports have followed [47]. Interestingly, the Sharma paper also points out that the water splitting reaction (reduction of water to hydrogen by reduced ceria) is thought to be a step in the mechanism for steam reforming over a ceria-containing catalyst.

Thus at the outset of this project, ceria and ceria-based materials were considered to be a strong candidate for CDS alongside the ferrites. And, as for the ferrites, it was assumed that the thermal reduction need not proceed to completion. That is, it is not necessary for the Ce_2O_3 phase to form; an oxygen deficient (partially reduced) ceria phase should suffice and may even be preferable (intermediate compositions between CeO_2 and Ce_2O_3 are known to form [48].) The simpler more general scheme is thus:

$$CeO_2 \rightarrow ODC + \tfrac{1}{2}xO_2$$
$$ODC + xCO_2 \rightarrow CeO_2 + xCO$$

Where ODC = Oxygen Deficient Ceria (CeO_{2-x} where $0 < x \leq 0.5$)

Bulk reduction of pure ceria is known to be difficult. That is, it is well-established that high surface areas (smaller particles) promote reduction of ceria [49]. Unfortunately, ceria is prone to sintering. Thus, from an engineering aspect, one approach for utilizing ceria for CDS may be the formation of a composite material with a non-reactive (or sparingly reactive) solid to maintaining high surface area and reactivity [50].

An alternative to engineered structures and composites for increasing reactivity and materials utilization is the chemical modification of ceria, i.e. the use of cerium compounds rather than pure ceria. Important properties including ease of reduction, bulk reducibility, and sintering resistance can all be manipulated and improved by the addition of dopants or by forming solid solutions. Thus mixed metal cerium oxides (MMCO) should be of great interest for the thermochemical splitting of CO_2 (and H_2O) according to the generalized reaction schemes:

$$MMCO \rightarrow ODMMCO + \tfrac{1}{2}xO_2$$
$$ODMMCO + xCO_2 \rightarrow MMCO + xCO$$
&
$$MMCO \rightarrow ODMMCO + \tfrac{1}{2}xO_2$$
$$ODMMCO + xH_2O \rightarrow MMCO + xH_2$$

Where MMCO = Mixed Metal Cerium Oxide and ODMMCO = Oxygen Deficient Mixed Metal Cerium Oxide.

In particular, solid solutions of ceria and zirconia are of interest as are rare earth and alkaline earth doped cerium oxides (yttrium doping is of particular interest), and ternary compounds of ceria, zirconia and alkaline earth or rare earth elements (again Y doping is of particular interest), although many other dopant, e.g. calcium, gadolinium and lanthanum have been studied and produce similar effects. As suggested for ferrites and pure ceria, it is likely not necessary to fully reduce the ceria to carry out the desired reactions. Further, it may not be desirable as phase changes are typically associated with volume changes that could induce cracking and failure in monolithic parts, or possibly unfavorable changes in reactivity and reversibility. On the other hand, certain cyclic redox treatments may enhance the materials' performance (see below). Below, we review some of the basics of cerium compounds.

One measurement of the ability of a material to cycle between oxidation states that is often applied to ceria-based materials is the oxygen storage capacity. This can either be a determination of only the most labile oxygen (OSC) or of the complete degree of reducibility of the solid (OSCC) [51]. It seems clear that the OSC or the OSCC is of relevance to the efficacy of ceria for CO_2 splitting. The OSC of pure ceria degrades at temperatures greater than 850 ºC due to particle sintering [52]. This is an indication that the OSC of pure CeO_2 is a surface dominated phenomenon. Dopants tend to stabilize the material against sintering, and the formation of solid solutions of ceria and zirconia is considered to be one the more effect ways to inhibit sintering. Although zirconium is isovalent with ceria, it has the additional effect of increasing the diffusivity of oxygen in the material by about 2 orders of magnitude for compositions in the range $Ce_{1-x}Zr_xO_2$ with $0.2 < x < 0.5$ This in turn has the effect of increasing the OSC as it becomes a bulk rather than solely a surface phenomena. In fact it has been reported that the OSC of CeO_2-ZrO_2 solid solutions is independent of surface area, even at moderate temperatures [53,54]. This results from defects introduced by variations in the cell parameters.

Yttrium is not isovalent with ceria and the effect of introducing yttrium into ceria to form yttria-doped ceria (YDC) is in part similar to that for zirconia to form yttrium-stabilized zirconia (YSZ). Namely, the introduction of the lower valent cation (Y(III)) introduces vacancies into the lattice resulting in enhanced ionic conductivity; (Under oxygen, i.e. when the ceria is fully oxidized, the ionic conductivity greatly dominates the overall conductivity [44].) Ionic conductivity of course relates to oxygen transport in the lattice and is thus of relevance to bulk reduction of the ceria. The conductivity has a maximum in the range of 3-5 mole % Y_2O_3, but remains high over about 2-10 mole % [55]. The ionic conductivity of YDC is reported to be greater than that of YSZ. In general for doped ceria the diffusivity of oxygen varies with stoichiometry and temperature; it can vary over several orders of magnitude with temperature. The specific dopant, e.g. Y, La, or Ga generally has only a small effect on the diffusivity. Ni/YDC catalysts have been reported to have higher activities for CO formation for dry reforming of methane if they are calcined at higher temperatures [56]. The introduction of Y, La and Ga along with zirconia to form ternary oxides has been reported to give improved results (lower reduction temperatures) over the binary ceria-zirconia solutions [57]. In contrast to these

reports, sintering of a doped ceria electrode on an YSZ electrolyte at temperatures > 1200 ºC is reported to form a reaction zone with limited ionic conductivity.

Solid solutions of ceria and zirconia exhibit complex phase behavior. For $Ce_{1-x}Zr_xO_2$ solid solutions with $x < 0.2$ (high ceria content), a cubic phase is formed, while for $x>0.8$ (high zirconia content), a monoclinic phase is formed. For the range $0.2<x<0.8$ there are numerous stable and metastable phases, with at least three tetragonal phases being identified. Thus, the phases present in a sample can be history dependent. For example, for materials of composition $Ce_{1-x}Zr_xO_2$ where $0.4<x<0.6$ reduction at high temperature (1000-1523 K) followed by oxidation at intermediate temperatures (700-873 K) is reported to alter subsequent redox behavior and dramatically increase OSC. This is an indication that different reduced phases are stable at different temperatures, and the identity of the reduced phase impacts the phase that is formed upon reoxidation.

As a specific example, when the stable t' tetragonal phase of $Ce_{0.5}Zr_{0.5}O_2$ is reduced with H_2 at temperatures > 1323 K, a cubic pyrochlore phase ($Ce_2Zr_2O_7$) is formed. (The pyrochlore phase tends to segregate to grain boundaries and induce electronic conductivity [49].) At lower temperatures, a CaF_2-related cubic phase is formed. On reoxidation at 700-873K metastable cubic k and t'_{meta} phases are formed. Because these phases are metastable, it is easier to remove the oxygen from them during subsequent cycling. In contrast, if the pyrochlore phase is reoxidized at high temperature, a more stable t* tetragonal phase can form. In this case the oxygen becomes more difficult to remove [52]. Even without reduction, the solid solutions appear to evolve with high temperature aging. For example it has been reported that partial demixing of the solution occurs across the composition range upon aging at 1473 K and that new phases of approximate composition $Ce_{0.8}Zr_{0.2}O_2$ and $Ce_{0.12}Zr_{0.88}O_2$ form, although surface enrichment of neither of the elements is observed [58].

As already indicated the phases formed upon reduction add additional complexity. As the Ce(IV) in the CeO_2-ZrO_2 system is reduced to Ce(III), the operative system eventually becomes Ce_2O_3-ZrO_2. For the Ce_2O_3-ZrO_2 system, the previously mentioned pyrochlore phase, $Ce_2Zr_2O_7$, is stable for 44-57 mol% $CeO_{1.5}$. In the zirconia rich region (3-44%) the pyrochlore is in equilibrium with a monoclinic Ce_2O_3-ZrO_2 solution at temperatures less than 1273 K, and in equilibrium with a tetragonal Ce_2O_3-ZrO_2 solution at higher temperatures. In the ceria rich region (57-81%) the pyrochlore is in equilibrium with a cubic phase. The cubic phase is stable from 81-85% $CeO_{1.5}$ [59]. Yttria in higher concentrations can suppress the formation of the pyrochlore phase from the cubic phase on reduction [60].

2.2 Accomplishments

2.2.1 Proof of Principle

Figure 4 illustrates and compares water and carbon dioxide splitting over two nominally identical 1.6 g robocasted monolithic lattice structures composed of a cobalt ferrite composition mixed with yttria stabilized zirconia (YSZ) in a 1:3 ratio by weight. In each case the material was thermally reduced at 1400 ºC in flowing inert gas for several hours. Following reduction, the temperature was lowered to 1100 °C and then CO_2 (5% in He

flowing at 55 sccm total) or water (50 sccm Ar saturated with steam at 80-90 °C) was fed over the monolith to produce CO or H_2 as shown in the figure. O_2, CO, and H_2 levels in the reactor effluent were quantified by gas chromatography (after a water condensation step). This sequence was repeated over seven cycles for the CDS case. For the WS case, 31 cycles were completed with some variations in reaction times and temperatures. Data for cycles 1-4 in the CDS case is not shown due to problems with O_2 leakage into the system. For WS, only cycle 5 is shown for comparison to CDS; at this point the histories of each sample were similar. CDS over the ferrite is very similar to WS with an initial rapid conversion followed by a slow decline. Despite the lower concentration of CO_2 in the reacting gas, yields are comparable, as is the general observation (which requires confirmation) that product yield increases with cycling (not shown here for WS).

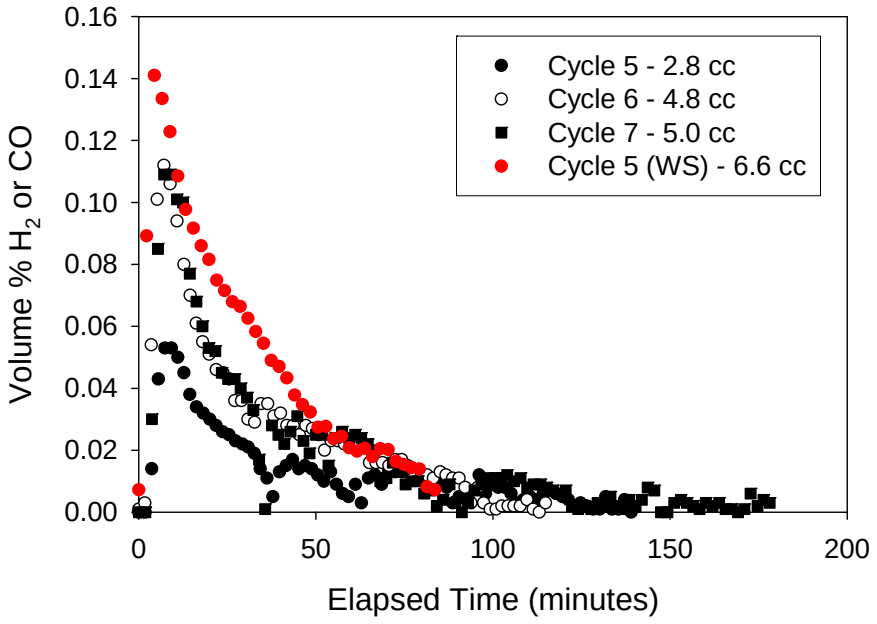

Figure 4. CDS and WS over robocast monolith of composition 1:3 $Co_{0.67}Fe_{2.33}O_4$:YSZ by weight. Gas yields are normalized per gram of ferrite (not monolith).

Figure 5 illustrates WS and CDS over a ceria/zirconia composition. The experiments were similar to those described above, however, in this case, a single 2.2 g pressed disk (nominally 50% porous) was utilized. Four cycles of WS (cycle 3, typical of the others is shown) and a single cycle of CDS (with 10 and 20% CO_2 in He) were carried out over this composition. Two other compositions were also tested $Ce_{0.5}Zr_{0.5}O_2$ and $Ce_{0.75}Zr_{0.25}O_2$. In general, we observed that high ceria content provided very high and thus more promising oxygen yields, but extensive sintering of thee samples resulted in a total loss of porosity and subsequent reactivity. Monolithic structures comprised of large scale open networks would be one approach to alleviating this problem. Nonetheless, Figure 5 demonstrates, we believe for the first time, that both cyclic WS and CDS proceed over ceria/zirconia at reasonable CSP temperatures.

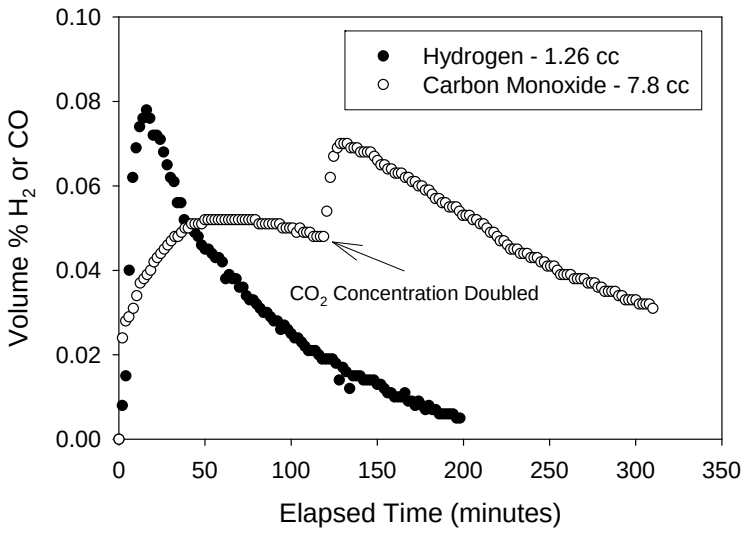

Figure 5. CDS and WS over porous disk with nominal composition of $Ce_{0.25}Zr_{0.75}O_2$. Yields have not been normalized.

A comparison of Figure 4 and Figure 5 offers some insight into the WS and CDS processes. In particular it appears that in Figure 1 that the rates of WS and CDS are somewhat similar, while in Figure 2 it is clear that the processes are very different. The data in Figure 4 and the data for WS in Figure 5 is consistent with a scenario in which the initial reaction rates are surface limited followed by a regime in which the reaction rates rapidly decline as surface sites are consumed (the surface is oxidized) and transport away from the surface and into the bulk must take place. The close similarity in the profiles suggests that the reactions very quickly become bulk transport limited so that differences in the inherent surface reaction rates for CO_2 and H_2O are quickly masked by transport. Rapid reactions with low levels of background O_2 may also be playing a role as the yields of both H_2 and CO in these three cases tend to be less than one would expect based on O_2 yields during the reduction steps (not shown).

The case for CDS over ceria/zirconia is more complex. Utilizing CO_2 does not require the use of heat tracing. This has proven to result in improved leak-tightness of reactor seals. Thus, as seen, the yield of CO is greater than the yield of H_2. It is also more consistent with expectations based on O_2 yields. The slow increase, relative to the other cases, in CO concentration in the effluent over time is an indication that the surface reaction rate is not only relatively slow, but is also responding to the degree of reduction, that is, this behavior does not result from dispersion in the flow system. The relatively slow decrease after the maximum is reached is an indication that the rate of CDS in this regime is limited by surface reactions. Both of these assertions are supported by the fact that the conversion responds rapidly to an increase in the concentration of CO_2 in the feed stream. The limited reaction rate of CO_2 over the ceria-based material may well results from the lack of a metal or metal ion capable of catalyzing C-O bond cleavage. In other words, the results could be improved if a suitable catalyst or catalytic function could be incorporated into the ceria formulations.

2.2.2 On-Sun Verification

To verify laboratory results, CDS was carried out over multiple cylindrical lattice-structured monolithic samples of $Co_{0.67}Fe_{2.33}O_4$ mixed with YSZ (1:3 and 1:5 by weight) at the national solar thermal test facility (NSTTF). During typical operations the samples were thermally reduced at about 1500 ºC for 10 minutes in an inert He atmosphere flowing at 120 sccm through the lattice. Following reduction, temperatures were reduced from 1500 °C to 1100 °C over the course of 1-2 minutes. The helium flow was then stopped and undiluted CO_2 was introduced at a flow rate of 120 sccm. The CO_2 flow was continued for 10 minutes, then He was re-introduced and the cycle was repeated. Temperatures were controlled by adjusting the incident flux level via the furnace attenuator, a shutter that moderates the amount of light reaching the primary parabolic concentrator mirrors, and measured using a Mikron pyrometer. O_2 and CO were quantified in the reactor effluent at 80 second intervals using a micro gas chromatograph equipped with a mol-sieve column and TCD detector. Results for a test conducted with a 3 g sample (0.5 g of ferrite) showing typical features are presented in Figure 6 along with a photograph of a typical monolith prior to testing.

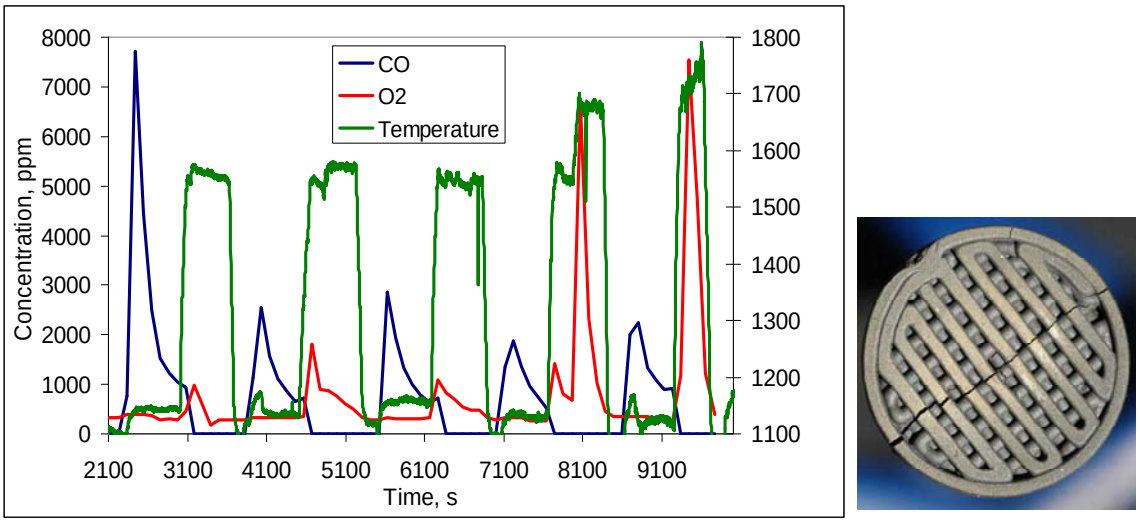

Figure 6. Demonstration of solar-driven cyclic production of O_2 and CO from CO_2 over a $Co_{0.67}Fe_{2.33}O_4$/YSZ monolith. Also shown is a typical monolith sample (16 mm dia.) of Co-ferrite and YSZ prior to testing

Several observations can be made upon examination of Figure 6. First, the CO peak from the first cycle is considerably larger than the successive peaks. This has also been observed by us in WS using Co-ferrite, and it likely resulted from the sample being more uniformly and more highly reduced prior to testing.

Second, O_2 and CO_2 are both produced during each successive cycle. Also, although compressed, the shapes of the product curves are similar to those in Figure 4, and are consistent with an initially rapid surface reaction followed by slower bulk processes. These two facts verify that the system is indeed acting as a thermochemical cycle. Finally, note that the temperature of the thermal reduction step has a significant impact on the amount of O_2 produced. This is evident in the 4th reduction cycle (1700 ºC), and the 5th cycle (1800 ºC) wherein it was our intention to push the sample to failure.

Although it is not evident from Figure 6, the extreme temperatures of the 4th and 5th cycles ultimately resulted in sample failure. An optical camera equipped with a zoom lens and the appropriate filters recorded partial melting occurring at about 1700° C. As the temperature was increased further, a secondary failure mechanism, chemical reaction of the Co-ferrite with the mullite tube in which it was supported, was also observed.

2.2.3 Demonstration of Short Cycle CDS

Practical thermochemical reactors such as the CR5 heat engine under development at Sandia [22] will require relatively short cycle times, e.g. on the order of minutes. With this in mind a solar test reactor with was designed and built with minimum dead volume to minimize gas switching times, dispersion and thermal mass, and wherein the reactive material samples were heated directly with concentrated solar energy to allow for very rapid heating and cooling (Figure 7). Product gases were analyzed with a non-dispersive infrared (NDIR) analyzer that provides a sensing response time of about five seconds to reach full scale. The combination of rapid heating and cooling along with the response time of the NDIR analyzer makes it possible to collect data more relevant to fielding a practical system.

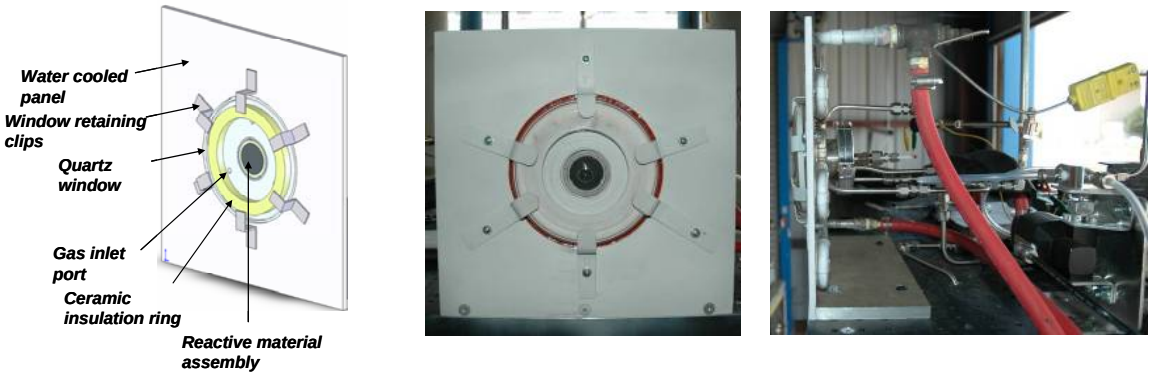

Figure 7. Schematic, front, and side views of advanced reactor for evaluating monolithic samples.

Data collected for a 30 g cobalt ferrite monolith with this system is shown in Figure 8. The gas flow rate of helium (during thermal reduction) and CO_2 (during oxidation) was held constant at 1 slpm. The figure shows CO production data (concentration) for several reactions ranging in duration from a maximum of two minutes to a minimum of one minute. The midplane reactant temperature is plotted on a secondary axis measured with a thermocouple inserted from the back (dark-side) of the sample. The illuminated surface temperature was at least 100 °C higher than the thermocouple temperature. Figure 8 shows that the baseline cobalt ferrite material is capable of repeatable CO_2 decomposition reactions with a reaction time of one minute or more. The data also indicate, based on the shape of the CO concentration profile, that the initial reaction rate is unaffected by a decrease in thermal reduction duration from two minutes to one minute.

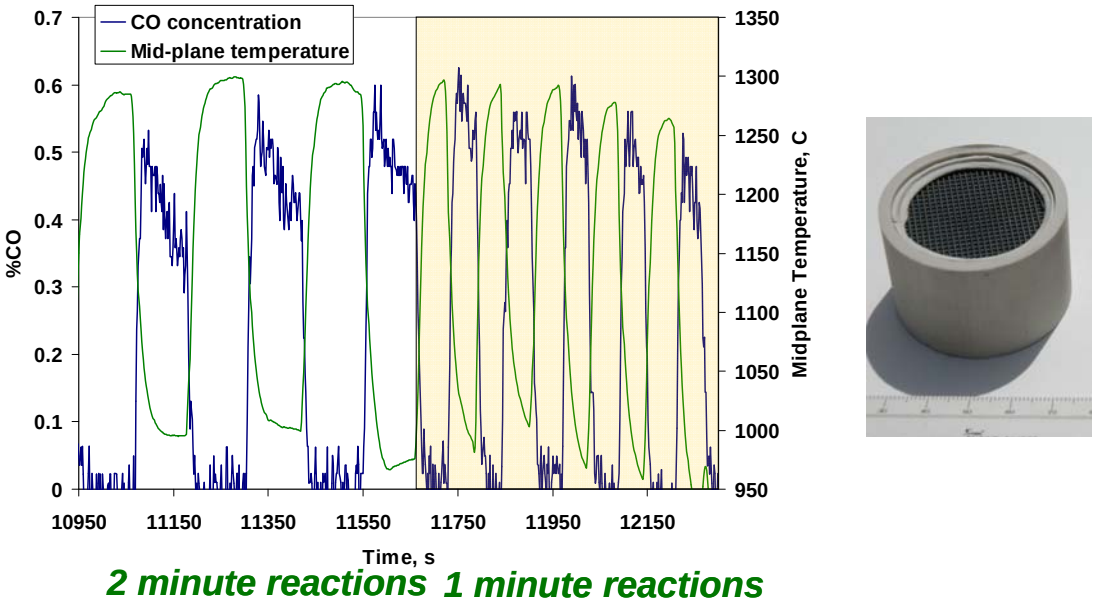

Figure 8. Carbon monoxide production and cycle temperature for on-sun testing of a 30 g robocast cobalt ferrite monolith ($Co_{0.67}Fe_{2.33}O_4$:YSZ, 1:4 by weight.) Photograph shows typical as-prepared monolith mounted for testing.

2.2.4 Improvements in Monolith Design and Material Utilization

One of the requirements for achieving optimal utilization of the solar resource and the reactive monolith is to maximize the contact between the solar flux and the reactive material. Line-of-sight access is advantageous because heat transfer by direct thermal radiation is much faster than conduction and convection. Our robocast samples typically consist of several layers of extruded rods that are nominally 1 mm in diameter and spaced by 1 mm (see Figure 8). With this geometry the degree of direct light penetration is limited to the first 2 mm of the sample which is generally over 8 mm thick. It is reasonable to expect then that much of the sample is not being fully utilized. That is, although a significant fraction of heat flows to the back side of the sample, in a short cycle test the temperature of the dark regions remains lower than is necessary or at least is optimal. This underutilized material leads to a performance penalty as it would in a real system. The degree of underutilization of the standard reactive monoliths was evaluated by comparing the performance of 8 mm thick Robocast samples to that of a 1.2 mm thick sample that was cut from a larger one using a diamond saw. The penalty is made obvious by normalized gas yields to the ferrite content of the sample.

The reaction tests were made in an upgraded version of the low volume solar reactor shown in Figure 7. CO and CO_2 were measured using an NDIR gas analyzer and O_2 was measured with a paramagnetic sensor, both from California Analytical. The temperature of the sample was measured using an infrared pyrometer from IMPAC that is sensitive to thermal radiation centered at 1.39 microns. Measurement at this wavelength allows the pyrometer to see through quartz glass and also to be blind to reflected solar radiation since the measurement is within an atmospheric water absorption band. Results for the1.2 mm sample are shown in Figure 9. The front surface temperature during thermal reduction was roughly 1600 °C and 1200 °C for CO_2 oxidation. The ratio of CO to O_2

produced throughout the experiment is a bit high at 2.48:1. This can be explained by the relative response times of the NDIR and paramagnetic sensors. Due to some aftermarket modifications the paramagnetic sensor has a slower response time and likely does not measure all of the O_2 evolved during thermal reduction.

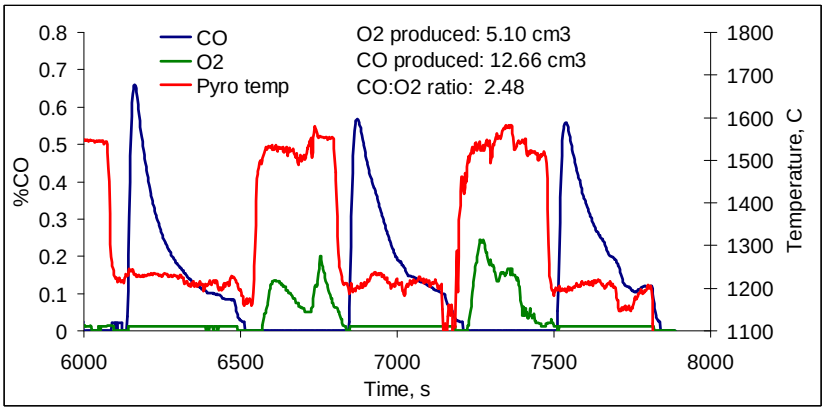

Figure 9. Temperature, and CO and O_2 production (instantaneous and integrated over test period) over thin (~1.2 mm) cobalt ferrite monolith ($Co_{0.67}Fe_{2.33}O_4$:YSZ, 1:2 by weight, 3.9 gram total.)

A comparison of the 1.2 mm sample to previously tested 8 mm samples is shown in Figure 10. The data for the 1.2 mm sample and the 8 mm samples were taken on two different NDIR devices, hence the difference in the "noise" of the traces. The 1.2 mm sample, having considerable less mass than the others, produced almost the same amount of CO. This leads to a considerable boost in performance on a specific CO production basis. Indeed, the reaction extent for the thinner, lighter sample was at least double that of previously tested materials, indicating a considerable increase in material utilization. The initial reaction rate of the 1.2 mm sample was larger than the others primarily due to 1) increased heat deposition rate resulting from line-of-sight through the entire structure and 2) a faster thermal response for the less massive sample. The reaction rate and shape of the production curves after 200 seconds is similar for all three materials suggesting a shared rate limiting mechanism, perhaps diffusion within the solid material.

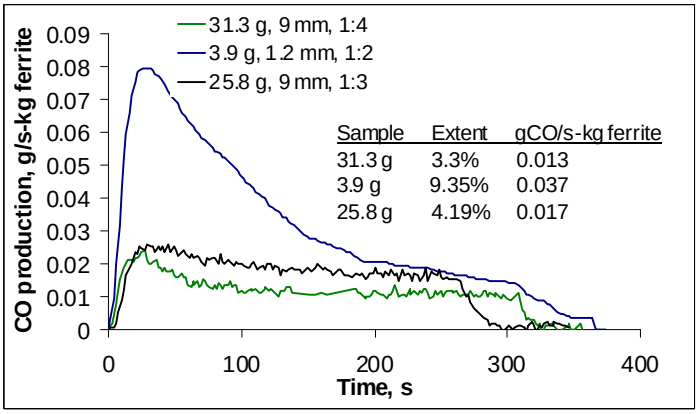

Figure 10. Comparison of CO production over a 1.2 mm thick cobalt ferrite monolith to that over two 8 mm thick samples under similar conditions. Relative ratios of cobalt ferrite and YSZ vary as shown in legend.

The results indicate that substantial performance gains can be made through an optimization of the reactive structure itself. A proposed advanced structure composed of an arrangement of vertical pins made from the reactive ceramic material is shown in Figure 11. This type of structure offers flexibility with respect to pin diameter, spacing, and height, making it well suited to carrying out a design optimization using empirical data and computational models. Ideally, these structures could be made with pin diameters as low as 100 microns. This, however, presents a challenge with respect to fabrication that we are planning to address using techniques previously developed at Sandia.

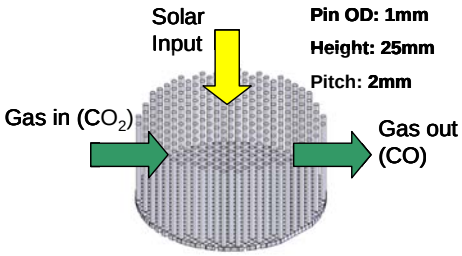

Figure 11. Proposed reactive monolith pin structure.

Throughout this section, results have been presented for cobalt ferrite monoliths constructed with varying ferrite:YSZ ratios. This was the result of early attempts to set bounds on ferrite loading in terms of performance and processability. The impact of ferrite loading on materials utilization was systematically addressed by robocasting a series of $Co_{0.67}Fe_{2.33}O_4$/YSZ monoliths with ferrite:zirconia weight ratios of 1:10, 1:5, 1:4, 1:3, 1:2, and 1:1.75. A 1:3 sample with 8% Y_2O_3 stabilized zirconia (as opposed to the standard 3%) was also fabricated. The $Co_{0.67}Fe_{2.33}O_4$ in each sample was all taken from the same large batch of material. The monoliths were each subjected to a mix of up to 11 standard and alternate water splitting (WS) cycles. No patterns emerged in ferrite utilization efficiency; differences between the samples were generally within the range of cycle to cycle variability typically seen, with one exception. The sample with the highest ferrite loading (1:1.75 by weight) appeared to lose activity with cycling; the final standard cycle over this sample, the eleventh cycle overall, produced only half the H_2 of the first cycle. It may be significant that this material should be bi-continuous with the ferrite forming a percolating network rather than existing as isolated particles in an YSZ matrix. One might expect the positive support effect to diminish at high ferrite loadings, particularly once the ferrite particles can form a continuous phase.

2.2.5 Demonstration and Characterization of Alternate Materials

Thermodynamic calculations recently performed at Sandia indicate that the ideal substitution level of alternate cations into the ferrite is at or near the stoichiometric amount, i.e. $M_xFe_{3-x}O_4$, $0.95 \leq x \leq 1$ [23]. Hence, thermal reduction, water splitting, and carbon dioxide splitting reactions for fine powder samples of $Co_{0.95}Fe_{2.05}O_4$ (CF), CF/3YSZ and CF/ZrO_2 were evaluated by TGA and XRD. Although the experimental methods require additional refinement to remove ambiguity, some general observations can be made: (1) At 1400 °C the reduction kinetics are slow. Higher temperatures were

beyond the current capabilities of the instrument. (2) FeO and/or CoO are present in the reduced CF sample by XRD. This is also seen in the ZrO_2-supported sample, but the region of interest is obscured for YSZ. No evidence of FeO/CoO is seen after water or CO_2 cycles in any of the samples, though there appears to be a change in the CF lattice parameter. (3) XRD of the 3YSZ-supported material shows that the YSZ is tetragonal. Upon reduction, a mixture of tetragonal YSZ and monoclinic ZrO_2 is present. (4) For all samples, oxidation via CO_2 at 1100 °C is kinetically faster and the extent is greater than for water vapor. (5) For the CO_2 oxidation, the kinetics for all three samples appears to be virtually instantaneous. It's difficult to discern any difference in a rate between the samples. An interesting feature to point out is that after the initial weight gain, both the ZrO_2 and YSZ samples show a small but noticeable weight loss under the CO_2 dwell (approx. 0.03-0.06%). This was not observed in the pure CF sample. (6) For the water splitting reaction, the kinetics differed slightly. The CF looks to have a much slower oxidation reaction than the supported samples. Thermogravimetric and X-ray diffraction studies of these and related materials are further discussed in a separate report [61].

An alternate approach to ferrite monolith construction and composition has been evaluated in the laboratory. Monoliths were fabricated from a simple physical mixture of as-purchased Fe_2O_3 (5 or 10% by weight) and YSZ. This approach eliminates the steps of synthesizing the mixed metal ferrite and milling the as-synthesized powders to an appropriately small particle size for monolith fabrication (generally < 10 microns). The Fe_2O_3/YSZ materials are extraordinarily easy to fabricate, and appear to be very robust. Samples have been tested for up to 49 cycles with no sign of chemical or physical degradation. It is thought that some of the Fe in these materials dissolves into the YSZ creating a new, and uniform active material. The formation of this phase over time could account for the improvement typically observed in our cobalt ferrite YSZ composites.

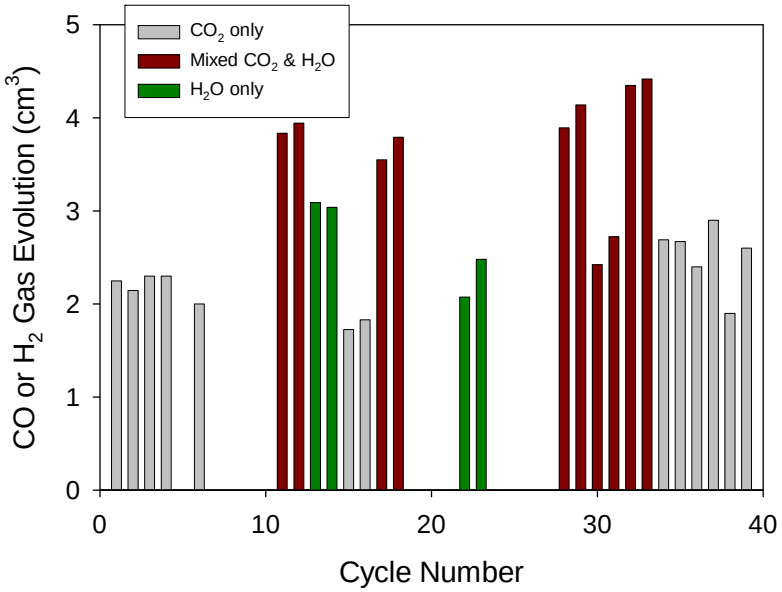

Figure 12. Gas yields for CDS, WS, and CDS+WS over a 2.8 g 5% Fe_2O_3/YSZ monolith; Thermal reduction at 1425-1450 °C, oxidation at 1100°C.

Figure 12 shows typical results obtained with a 5% Fe_2O_3/3YSZ composite under similar conditions for WS (green), CDS (gray), and mixed tests in which CO_2 was diverted

through a water bubbler at 40 °C upstream of the reactor (brown). These results suggest that there is a synergistic effect of unknown origin in the mixed system. That is, yields are higher in the mixed system. Figure 13 illustrates this further. In this case a standard CDS cycle was carried out, but after the CO evolution slowed, the CO_2 feed to the reactor was diverted to the bubbler. As can been seen in the shaded portions of the figure, CO production increased whenever both CO_2 and H_2O were present.

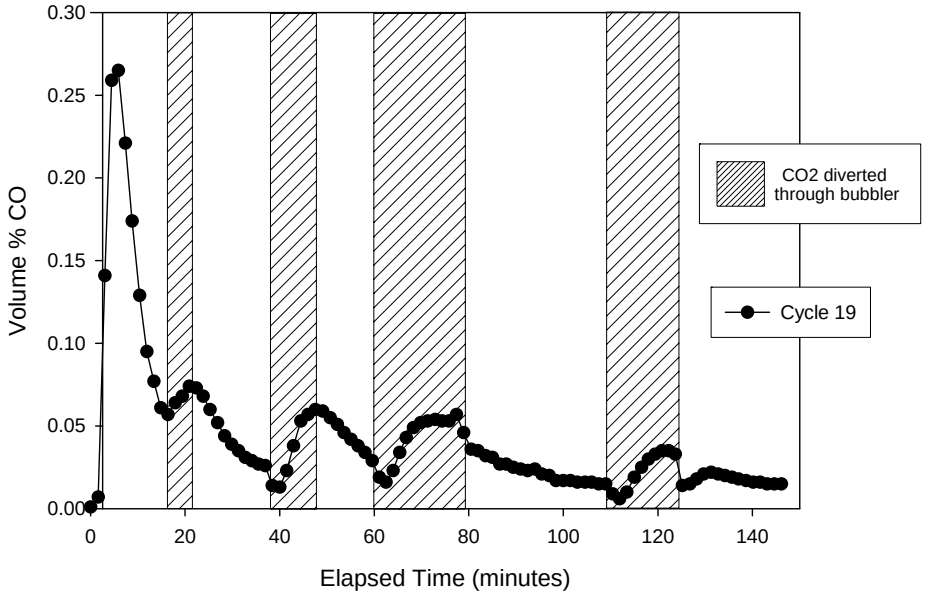

Figure 13. The effect of co-feeding water with CO2 during a single cycle over a robocast 5% Fe_2O_3/YSZ monolith.

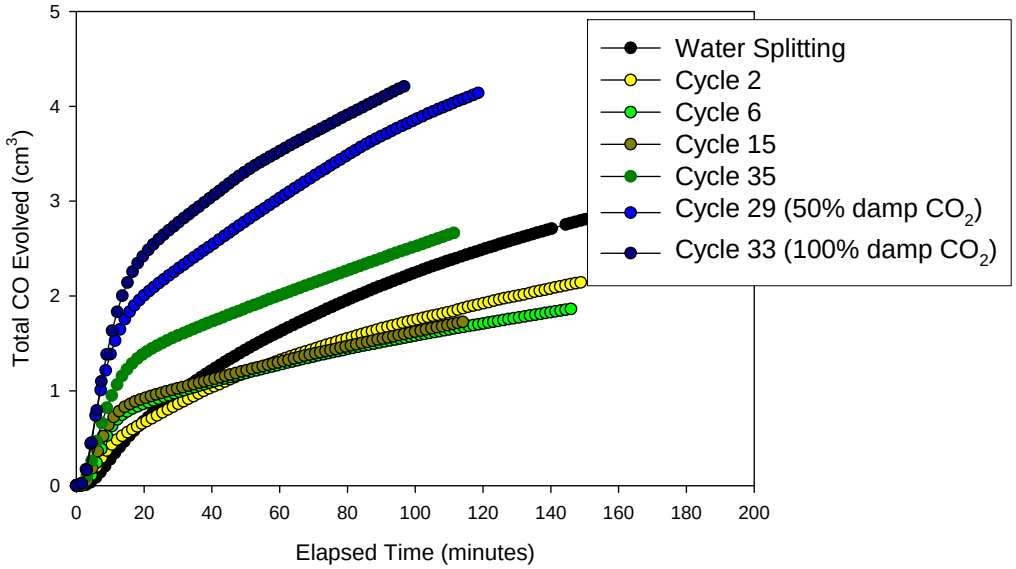

Figure 14. Gas evolution curves for various cycles and feed conditions (5% Fe_2O_3/YSZ monolith.) Feed gas was 80% CO_2 except as noted in legend.

Figure 14 shows several of the detailed gas evolution curves over the same monolith. It is clear from the figure that CDS is significantly faster than WS, consistent with the TGA results for the cobalt ferrite formulations. Additionally, the figure illustrates the improving performance with cycling (compare cycles, 2, 6, 15, and 35). The plot also shows that there are two separate regimes for the CDS reaction: an initial rapid reaction followed by a slower reaction. The most obvious explanation is an initial surface reaction process followed by a bulk transport/reaction process. Additional characterization and modeling is required to fully establish that this is the mechanism. Finally, the figure illustrates the improvement observed when water was co-fed with the CO_2. In cycle 29, the CO_2 concentration was decreased from 80% to 50%, however, the initial rate and the overall yield still showed significant improvement. Further improvements were realized upon feeding undiluted CO_2 saturated with water at 40 °C (cycle 33). The synergistic effect seen when cofeeding water and CO_2 has been reproduced over two additional samples comprised of 10% Fe_2O_3/YSZ. The origin of this effect is not well understood.

As previously stated, the improvement with cycling observed for Fe_2O_3/YSZ monoliths is consistent with the possible formation of active phases via reaction of Fe and YSZ. Temperature programmed reduction (TPR, sample temperature is ramped in flowing hydrogen and H_2 concentration is measured at outlet) of a typical Fe_2O_3/YSZ monolith are presented in Figure 15. The as-prepared sample displays a low temperature reduction peak (~ 350 °C) that is consistent with the presence of at least some Fe_2O_3. This peak is absent following a high temperature calcination procedure. This is consistent with the expected conversion of Fe_2O_3 to Fe_3O_4 and the observation that the sample converts to a uniform black color. The reduction curves flatten and shift to higher temperatures after CDS has been performed over the sample. This further illustrates that the material continues to evolve in a chemical sense as it is used for CDS.

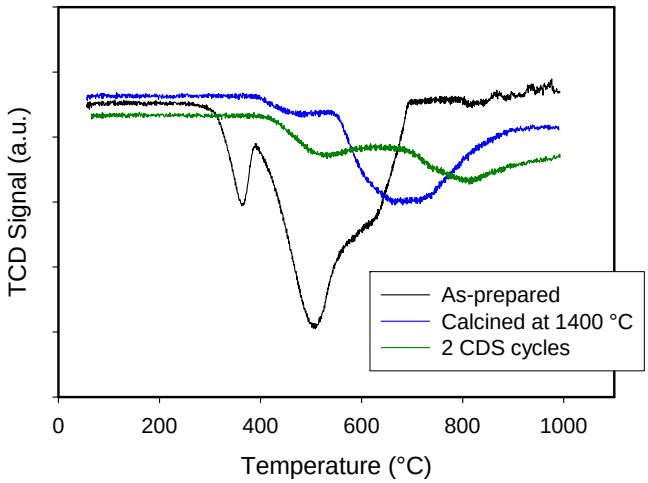

Figure 15. Temperature programmed reduction of 10% Fe_2O_3/YSZ monolith sample after various stages of preparation and use.

In order to further probe the interaction of Fe with ZrO_2 and YSZ, samples were prepared by co-precipitating varying amounts Fe with Zr and Y/Zr and calcined to 1100 °C to form Fe-doped ZrO_2 and Fe-doped YSZ (10% Y_2O_3, stabilized in the cubic form). A subset of these samples has been provided to Kodama's group in Japan for evaluation and will be

reported on elsewhere. XRD, TPR, and TPO (temperature programmed oxidation) evaluations of these materials were conducted at Sandia. The most interesting result came from oxidizing the H_2 reduced samples and is shown in Figure 16. The figure shows that the Y-containing samples were significantly easier to reoxidize than the ZrO_2 samples. (Little difference was seen for the reduction step.) Although intriguing, the significance of this result remains to be seen and should be viewed with caution for several reasons. First, the TPR is a "hard reduction" that at the very least will reduce "free" iron oxides to the metallic form rather than the more relevant wustite phase. Second, TPO is carried out with O_2 rather than CO_2 or H_2O and hence the thermodynamic driving forces are much different than those in thermochemical system.

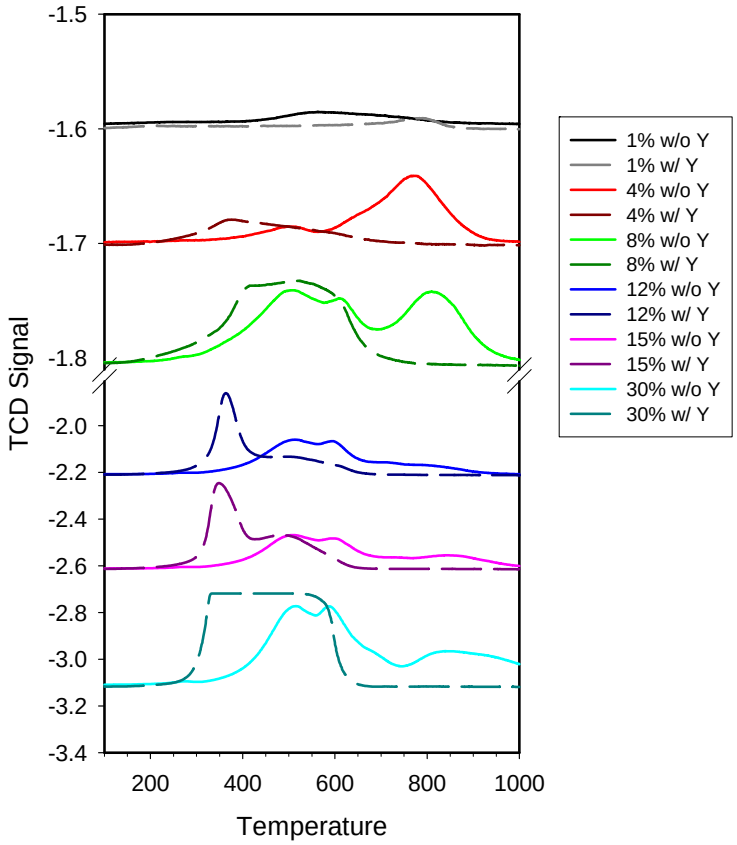

Figure 16. Temperature programmed oxidation of varying amounts of Fe co-precipitated with Zr or Y/Zr, calcined to 1100 °C and H_2 reduced.

Finally, work has continued on the ceria/zirconia formulations and combinations of WS and CDS has been carried over these materials for as many as 25 cycles. The best yields were realized over the $Ce_{0.5}Zr_{0.5}O_2$ formulation. Reduction temperatures as high as 1525 °C have been successfully used, and O_2 yields are observed to increase with temperature as expected. Unfortunately, oxidation of the reduced materials with CO_2 remains a slow process and thus CO yields tend to be smaller than expected based on O_2 yields. Since reoxidation is incomplete, O_2 yields tend to decrease on successive cycles. However, the initial levels can be restored by oxidizing the samples with O_2. Hence, the primary issue is not deactivation, but rather slow kinetics. The kinetics are such that CO yields are virtually zero at 1100 °C but increase to be more than the expected values at 1400 °C. At

1400 °C the rate of CO_2 thermolysis is sufficiently high that the reduced ceria is evidently acting as a getter of the O_2 produced by thermolysis. Thus the product mixture leaving the reactor in these cases contains a mixture of CO_2, CO, and ultimately the amount of O_2 that is produced in excess of the capacity of the reduced material. Efforts to couple catalytic metals to these materials have been only marginally successful to date. We have demonstrated that a noble metal catalyst promotes the CDS reaction over our materials at temperatures below 400 °C. However, these catalysts are not stable to thermal reduction temperatures. Attempts to incorporate more refractory materials, e.g. Fe and Ni, have not yet led to an increase in reaction kinetics to the desired level.

3.0 High Temperature Metal-Oxide Carbon Dioxide Splitting Cycles

The primary goal of this thrust was identifying and demonstrating high temperature CDS cycles that are compatible with both next-generation nuclear energy and concentrating solar power (maximum temperatures < 900 ºC). Examination of existing water splitting databases for cycles that might be adapted to CDS revealed no candidates that were judged to be realistic. Therefore, the effort proceeded to the laboratory discovery phase. Figure 17 shows thermal reduction profiles for CeO_2, and several Ce/Zr and Y/Ce/Zr oxide compositions synthesized by standard coprecipitation methods (for clarity, legend shows only the ratio of metals in the sample, omitting the oxygen.) As discussed previously, it is known from the catalyst literature that a 1:1 ratio of Ce:Zr produces the best oxygen storage materials, and that Y can improve transport and storage capacity as well. Indeed, Figure 17 illustrates that a material with a composition of $Y_{0.1}Ce_{0.45}Zr_{0.45}O_{1.95}$ liberates O_2 over a temperature range of about 100-1050 ºC. The reoxidation of the thermally reduced material with oxygen was also verified (Figure 18.) The overall extent of reduction was small, and similar formulations were found to be stable under these conditions.

This aspect of the project was not continued into the second year for several reasons. First, water splitting is more thermodynamically favorable than CDS at temperatures below about 800 °C [20]. Second, basic thermodynamic considerations indicate that the thermochemical approach to this chemistry may well require ultra-high temperatures if the cycle is to be limited to two steps involving metal oxides [62].

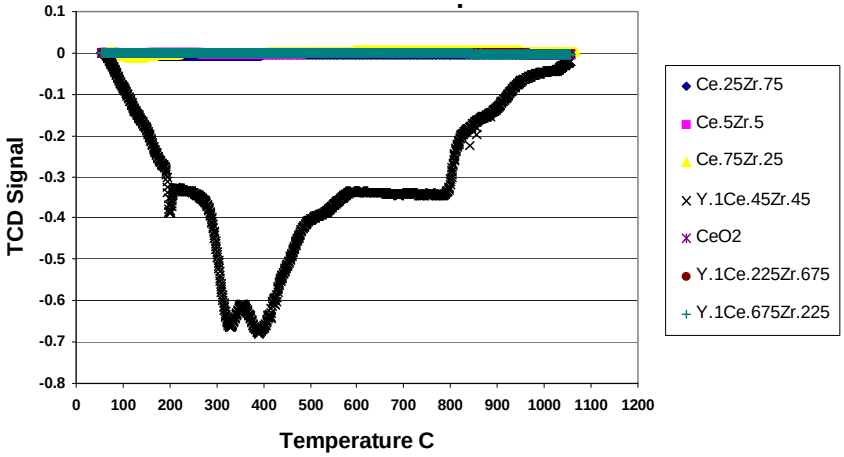

Figure 17. Temperature programmed reduction of ceria/zirconia powders in flowing inert gas.

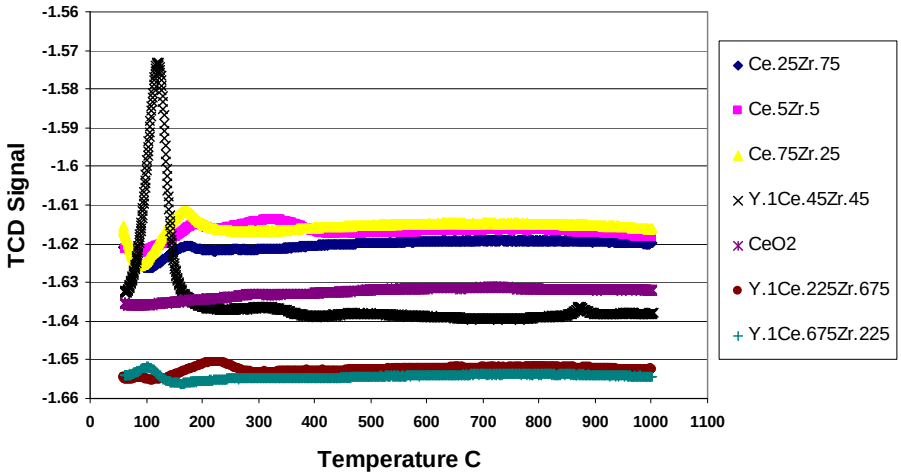

Figure 18. Temperature programmed oxidation of thermally reduced ceria/zirconia powders.

4.0 Automated Discovery of New Carbon Dioxide Splitting Cycles

In this thrust we developed a code that was linked to the HSC thermodynamic database of over 5000 compounds. We then used this code to exhaustively search for cycles that are of the form:

$$AO \rightarrow A + \tfrac{1}{2} O_2$$

$$A + CO_2 \rightarrow AO + CO$$

The code generated a total of 2,131 such cycles. This list was next screened by the code to identify the reaction pairs that are thermodynamically feasible, i.e. in which ΔG of each reaction step at a defined temperature is negative or small. The results of this process are summarized in Table 3. As expected, ceria is identified as a potential candidate. Less expected were the results for bismuth and arsenic oxides, although on closer inspection these reactions involve reactions of gaseous species and are likely not realistic.

Table 3. Potential Two-step CDS Cycles

Identified Cycle	ΔG (kcal/mole) (1600 °C)	ΔG (kcal/mole-CO2) (100 °C)
$2As_4O_9 \rightarrow 8AsO_2 + O_2$	-4	
$2CO_2 + 8AsO_2 \rightarrow 2As_4O_9 + 2CO$		-166
$2As_4O_{10} \rightarrow 8AsO_2 + 2O_2$	-10	
$4CO_2 + 8AsO_2 \rightarrow 2As_4O_{10} + 4CO$		-67
$4Bi_4O_6 \rightarrow 8Bi_2O_2 + 4O_2$	18	
$8CO_2 + 8Bi_2O_2 \rightarrow 4Bi_4O_6 + 8CO$		-13
$6Bi_4O_6 \rightarrow 8Bi_3O_4 + 2O_2$	6	
$4CO_2 + 8Bi_3O_4 \rightarrow 6Bi_4O_6 + 4CO$		-16
$4CeO_2 \rightarrow 2Ce_2O_3 + O_2$	14	
$2CO_2 + 2Ce_2O_3 \rightarrow 4CeO_2 + 2CO$		-18
$2In_2O_3 \rightarrow 2In_2O + 2O_2$	45	
$4CO_2 + 2In_2O \rightarrow 2In_2O_3 + 4CO$		-28
$2SnO_2 \rightarrow 2SnO + O_2$	20	
$2CO_2 + 2SnO \rightarrow 2SnO_2 + 2CO$		-1

The next step taken was to extend the method to three-step cycles and refine the method so that the output included the temperature where the ΔG of each reaction is approximately zero. The first step of each cycle is the CO producing reaction; the second step is the oxygen producing reaction. Thus CO_2 is introduced into the third step where it reacts with the non- CO and O_2 products of the first two reactions. More simply put, the reactions follow the sequence:

$$ACO \rightarrow A + CO$$
$$BO \rightarrow B + \tfrac{1}{2} O_2$$
$$A + B + CO_2 \rightarrow ACO + BO$$

This process produced 54 candidate reaction sequences. The highest temperature associated with any of these sequences is 998K. The first reactions identified principally fall in the category of metal carbonyl decomposition. The decomposition of phosgene and a radical reaction were also highlighted. Each one of the first reactions is provided in Table 4 along with the temperature where the reaction was calculated from the database to be spontaneous. Not surprisingly, for each of the initial reactions identified, the associated oxygen evolving reactions were generally drawn from a common set of reactions. This set included reactions of bismuth, cesium, hydrogen, iodine, and molybdenum oxides as well as the decomposition of sodium cyanate. The complete set of sequences involving phosgene is shown in Table 5 as an example. In general these

cycles appear to be impractical and again in many cases involve what would seem to be unrealistic reactions of metal-containing gas phase species.

Table 4. Candidate Reactions for Producing Carbon Monoxide.

CO Liberating Reaction	Temp (K)
$COCl_2 = Cl_2 + CO$	800
$Fe(CO)_5 = Fe + 5\ CO$	317
$Fe_2(CO)_9 = Fe_2 + 9\ CO$	713
$Mn(CO)_5Br = MnBr + 5\ CO$	579
$Mn(CO)_5I = MnI + 5\ CO$	607
$Mo(CO)_6 = Mo + 6\ CO$	369
$Os(CO)_5 = Os + 5\ CO$	877
$Ru(CO)_5 = Ru + 5\ CO$	922
$W(CO)_6 = W + 6\ CO$	335
HCO = H + CO (H and HCO radicals)	537

Table 5. Potential Three-step CDS Cycles Involving Phosgene Decomposition

Reaction Sequence	Temp (K)
$COCl_2 = Cl_2 + CO$	800
$Bi_2O_3 = 2\ BiO + ½\ O_2$	717
$Cl_2 + 2\ BiO + CO_2 = COCl_2 + Bi_2O_3$	375
$COCl_2 = Cl_2 + CO$	800
$½\ Cs_2O_4 = CsO + ½\ O_2$	968
$Cl_2 + CsO + CO_2 = COCl_2 + ½\ Cs_2O_4$	454
$COCl_2 = Cl_2 + CO$	800
$HO_2 = H_2O_2 + ½\ O_2$	465
$Cl_2 + ½\ H_2O_2 + CO_2 = COCl_2 + HO_2$	955
$COCl_2 = Cl_2 + CO$	800
$I_2O_5 = 2\ IOO + ½\ O_2$	678
$Cl_2 + 2\ IOO + CO_2 = COCl_2 + I2O5$	345
$COCl_2 = Cl_2 + CO$	800
$3\ Mo_3O_9 = Mo_9O_{26} + ½\ O_2$	832
$Cl_2 + Mo_9O_{26} + CO_2 = COCl_2 + 3\ Mo_3O_9$	978
$COCl_2 = Cl_2 + CO$	800
$2.25\ Mo_4O_{12} = Mo_9O_{26} + ½\ O_2$	773
$Cl_2 + Mo_9O_{26} + CO_2 = COCl_2 + 2.25\ Mo_4O_{12}$	938
$COCl_2 = Cl_2 + CO$	800
$1.8\ Mo_5O_{15} = Mo_9O_{26} + ½\ O_2$	760
$Cl_2 + Mo_9O_{26} + CO_2 = COCl_2 + 1.8\ Mo_5O_{15}$	937
$COCl_2 = Cl_2 + CO$	800
$NaCNO = NaCN + ½\ O_2$	900
$Cl_2 + NaCN + CO_2 = COCl_2 + NaCNO$	475

Taken as whole the results of the search suggest that ultrahigh temperature metal oxide cycles are most attractive and implementable approaches to thermochemical CDS.

5.0 Conclusion

Energy is by far the largest human endeavor on the planet; global expenditures measured roughly $3 trillion in 2005, or more than twice the amount spent on agriculture and 3 times the amount on defense [63,64]. Tremendous capital is invested in the current hydrocarbon infrastructure, however massive capital investments will continue to be necessary, even if we choose to preserve the fossil fuel paradigm. Applying renewable energy resources to recycle CO_2 is a new paradigm for storing and transporting energy that preserves much of the hydrocarbon infrastructure, while offering a more environmentally sound future. Thermochemical cycles for splitting water and carbon dioxide have promise as methods to realize this paradigm. CDS has been demonstrated over both iron- and ceria-based monolithic materials of the type required for a solar reactor such as the CR5. Carbon deposition is a possible concern for the Fe-based materials, however deposition of measureable quantities was not observed in this effort. This may be due to the high temperatures and relatively large excess of CO_2 employed in these studies. As work proceeds towards pushing the reactions to lower temperatures and higher conversions, this problem may yet present itself. Cofeeding steam with CO_2 is one potential solution. Alternately, ceria-based cycles appear to be attractive provided that the reaction kinetics can be improved. Future efforts should be directed towards understanding the reaction and materials chemistry of the Fe- and Ce-based systems, applying this information towards developing a new generation of materials, developing advanced structures and reactors, and conducting systems evaluations to determine the potential cost and viability of this approach.

6.0 References

1. U.S. Energy Information Administration, data available online at http://tonto.eia.doe.gov/country/country_time_series.cfm?fips=US

2. Stacy C. Davis, Susan W. Diegel, Robert G. Boundy "Transportation Energy Data Book: Edition 27" Chapter 1; Oak Ridge National Laboratory ORNL-6981, 2008; available online at http://cta.ornl.gov/data/tedb27/Edition27_Chapter01.pdf

3. David L. Greene and Sanjana Ahmad "Costs of U.S. Oil Dependence: 2005 Update" Oak Ridge National Laboratory Report ORNL/TM-2005/45, January 2005.

4. Michele Cavallo "Oil Prices and the U.S. Trade Deficit" Federal Reserve Bank of San Francisco Economic Letter Number 2006-24, September 22, 2006.

5. Justin Fox "The trade deficit has turned very oily lately" Time Magazine Online weblog, May 29, 2008; available online at http://curiouscapitalist.blogs.time.com/2008/05/29/the_trade_deficit_has_turned_v/

6. Steven Mufson "Oil Price Rise Causes Global Shift in Wealth" Washington Post, Saturday November 10, 2007.

7. U.S. Energy Information Administration, data available online at http://tonto.eia.doe.gov/country/index.cfm

8. R. James Woolsey and Anne Korin, "Turning Oil into Salt" National Review Online, September 25, 2007.

9. Council on Foreign Relations Independent Task Force Report No. 58, "National Security Consequences of U.S. Oil Dependency" John Deutch and James R. Schlesinger, chairs, David G. Victor, project director (2006).

10. Nathan S. Lewis and Daniel G. Nocera "Powering the planet: Chemical challenges in solar energy utilization" PNAS 103 (2006) 15729.

11. See for example the International Energy Agency Report: World Energy Outlook 2008.

12. Jeffrey S. Dukes "Burning buried sunshine: Human consumption of ancient solar energy" Climatic Change 61 (2003) 31.

13. Hamilton O. Smith, Robert Friedman, and J. Craig Venter "Biological solutions to renewable energy" National Academy of Engineering website: http://www.nae.edu/nae/bridgecom.nsf/BridgePrintView/MKUF-5NTMX9?OpenDocument

14. Xin-Guang Zhu, Stephen P. Long, and Donald R. Ort "What is the maximum efficiency with which photosynthesis can convert solar energy into biomass?" Current Opinion in Biotechnology 19 (2008) 153.

15. Carbon Management: Implications for R&D in the Chemical Sciences and Technology, National Academies Press, 2001.

16. Carbon Dioxide Recovery and Utilization, M. Aresta, ed., Kluwer Academic Publishers, Dordrecht, 2003

17. X. Xiaoding and J.A. Moulijn "Mitigation of CO_2 by Chemical Conversion: Plausible Chemical Reactions and Promising Products" *Energy and Fuels*, 1996, **10**, 305.

18. Chemical & Engineering News July 2, 2007

19. U.S. Energy Information Administration Report "Emissions of Greenhouse Gases in the United States 2004" DOE/EIA-0573 (2004).

20. James E. Miller "Initial case for splitting carbon dioxide to carbon monoxide and oxygen" Sandia Report SAND2007-8012, Sandia National Laboratories, December 2007.

21. D. Mignard and C. Pritchard "Process for the synthesis of liquid fuels from CO_2 and marine energy" Trans IChemE, Part A, Chemical Engineering Research and Design, 2006, 84(A9): 828–836.

22. R.B. Diver, J.E. Miller, M.D. Allendorf, N.P. Siegel, R.E. Hogan "Solar Thermochemical Water-Splitting Ferrite-Cycle Heat Engines" Journal of Solar Energy Engineering 130 (2008) 041001-1. 19 (2008) 153.

23. M.D. Allendorf, R. B. Diver Jr., N.P. Siegel, and J.E. Miller "Two-Step Water Splitting Using Mixed-Metal Ferrites: Thermodynamic Analysis and Characterization of Synthesized Materials" Energy & Fuels 2008, 22, 4115–4124.

24. T. Kodama and N. Gokon “Thermochemical cycles for high-temperature solar hydrogen production” *Chem. Rev.* **2007,** *107*, 4048.

25. M.D. Shroff, D.S. Kalakkad, K.E. Coulter, S.D. Kohler, M.S. Harrington, N.B. Jackson, A.G. Sault and A.K. Datye “Activation of precipitated iron Fischer-Tropsch synthesis catalysts” J. Catal. 156 (1995) 185.

26. Y. Tamaura and M. Tahata “Complete reduction of carbon dioxide to carbon using cation-excess magnetite” Nature **346**, 255 (1990).

27. K. Akanuma, K. Nishizawa, T. Kodama, M. Tabata, K. Mimori, T. Yoshida, M. Tsuji and Y. Tamaura “Carbon dioxide decomposition into carbon with the rhodium-bearing magnetite activated by H_2-reduction” J. Mater. Sci. **28**, 860 (1993).

28. T. Kodama, H. Kato, G.S. Chang, N. Hasegawa, M. Tsuji, Y. Tamaura “Decomposition of CO_2 to carbon by H_2-reduced Ni(ii)- and Co(ii)-bearing ferrites at 300 °C” J. Mater. Res. **9**, 462 (1994).

29. H. Kato, T. Kodama, M. Tsuji, Y. Tamaura and S. G. Chang “Decomposition of carbon dioxide to carbon by hydrogen-reduced Ni(II)-bearing ferrite” J. Mater. Sci. **29**, 5689 (1994).

30. Tsuji M., Yamamoto T., Tamaura Y., Kodama T., Kitayama Y. “Catalytic acceleration for CO_2 decomposition into carbon by Rh, Pt or Ce impregnation onto Ni(II)-bearing ferrite” Appl. Catal. A **142**, 31 (1996).

31. Masahiro Tabata, Yoshikazu Nishida, Tatsuya Kodama, Keisuke Mimori, Takashi Yoshida and Yutaka Tamaura “CO_2 decomposition with oxygen-deficient Mn(II) ferrite” J. Mater. Sci. **28**, 971 (1993).

32. Masahiro Tabata, Kazuhiro Akanuma, Ken'ichi Nishizawa, Keisuke Mimori, Takashi Yoshida, Masamichi Tsuji and Yutaka Tamaura “Reactivity of oxygen-deficient Mn(II)-bearing ferrites ($Mn_xFe_{3-x}O_{4-\delta}$, $0 \leq x \leq 1$, $\delta > 0$) toward CO_2 decomposition to carbon” J. Mater. Sci. **28**, 6753 (1993).

33. M. Tabata, H. Kato, T. Kodama, T. Yoshida, M. Tsuji and Y. Tamaura “CO_2 decomposition with mangano-wüstite” J. Mater. Sci. **29**, 999 (1994).

34. T. Kodama, M. Tabata, K. Tominaga, T. Yoshida and Y. Tamaura “Decomposition of CO_2 and CO into carbon with active wüstite prepared from Zn(II)-bearing ferrite” J. Mater. Sci. **28**, 547 (1993).

35. M. Tsuji, K. Nishizawa, T. Yoshida and Y. Tamaura “Methanation reactivity of carbon deposited directly from CO_2 on to the oxygen-deficient magnetite” J. Mater. Sci. **29**, 5481 (1994).

36. K. Nishizawa, H. Kato, K. Mimori, T. Yoshida, N. Hasegawa, M. Tsuji and Y. Tamaura “Methanation of carbon deposited directly from CO_2 on rhodium-bearing activated magnetite” J. Mater. Sci. **29**, 768 (1994).

37. Masamichi Tsuji, Hiroyasu Kato, Tatsuya Kodama, Shih Ger Chang, Noriko Hesegawa and Yutaka Tamaura “Methanation of CO_2 on H_2-reduced Ni(II)-or Co(II)-bearing ferrites at 200 °C” J. Mater. Sci **29**, 6227 (1994).

38. T. Yoshida, M. Tsuji, Y. Tamaura, T. Hurue, T. Hayashida and K. Ogawa “Carbon recycling system through methanation of CO_2 in flue gas in LNG power plant” Energy Conversion and Management 38, S443 (1997).

39. J.-S. Kim, J.-R. Ahn, C.W. Lee, Y. Murakami and D. Shindo "Morphological properties of ultra-fine (Ni,Zn)-ferrites and their ability to decompose CO_2" J. Mater. Chem. **11**, 3373 (2001).

40. H.C. Shin, S.C. Choi, C.S. Kim, O.-S. Joo, K.-D. Jung "Redox Behavior of Cu-ferrite for CO_2 decomposition" Studies in Surface Science and Catalysis **153**, 145 (2004).

41. H.C. Shin, J.H. Oh, B.C. Choi, and S.C. Choi "Design of an energy conversion system with decomposition of H_2O and CO_2 using ferrites" Phys. Stat. Sol. C **1**, 3748 (2004).

42. H. Katsumata, K. Matsushita, S. Kaneco, T. Suzuki, and K. Ohta "Reduction of carbon dioxide using metal powders" Studies in Surface Science and Catalysis **153**, 55 (2004).

43. S. Abanades and G. Flamant "Thermochemical hydrogen production from a two-step solar-driven water-splitting cycle based on cerium oxides" Solar Energy 80, 1611 (2006).

44. M. Mogensen "Ceria-based Electrodes" in Catalysis by Ceria and Related Materials , A. Trovarelli, ed., Imperial College Press, London (2002).

45. S. Sharma, S. Hilaire, J.M. Vohs, R.J. Gorte, H.-W. Jen "Evidence for oxidation of ceria by CO_2" J. Catal. **190**, 1999 (2000).

46. S. Bernal, G. Blanco, J.M. Gatica, C. Larese, H. Vidal "Effect of mild re-oxidation treatments with CO_2 on the chemisorption capability of a Pt/CeO_2 catalyst reduced at 500 ºC" J. Catal. **200**, 411 (2001).

47. See for example O. Demoulin, B.M. Navez, J.L. Mugabo, P. Ruiz "The oxidizing role of CO_2 at mild temperature on ceria-based catalysts" Appl. Catal. B **70**, 284 (2007).

48. For CeO_x, $1.714<x<2$, there is a continuum of non-stoichiometric oxides with fluorite related structures at temperatures > 685 °C. For $x < 1.714$, the phase diagram is dominated at higher temperatures by a $Ce_2O_{3+\delta}$ phase with the bcc cubic type-C rare earth oxide structure. A. Trovarelli "Structural properties and nonstoichiometric behavior of CeO_2" in Catalysis by Ceria and Related Materials , A. Trovarelli, ed., Imperial College Press, London (2002).

49. Temperature programmed H_2 reduction of ceria typically shows a low temperature and higher temperature regime. It is generally assumed that this results from a stepwise reduction of the surface followed by the bulk although a surface kinetic model could also explain the result if it is assumed that nanocrystalline and bulk ceria have different kinetic and thermodynamic properties. E. Aneggi, M. Boara, C. de Leitenburg, G. Dolcetti, A. Trovarelli "Insights into the redox properties of ceria-based oxides and their implications in catalysis" J. of Alloys and Compounds **408**, 1096 (2006).

50. Silica has been reported to form composites with ceria that lead to isolated ceria nanoparticles with high reactivities under certain conditions. E. Rocchini, A. Trovarelli, J. Llorca, G.W. Graham, W.H. Weber, M. Maciejewski, and A. Baiker "Relationships between Structural/Morphological Modifications and Oxygen Storage–Redox Behavior of Silica-Doped Ceria" J. Catal. **194**, 461 (2000). The formation of nanocomposites of ceria and silica and ceria and titania is also reported in B.M. Reddy, A. Khan, P. Lakshmanan, M. Aouine, S. Loridant, and J.-C. Volta "Structural Characterization of nanosized CeO_2-SiO_2, CeO_2-TiO_2, and CeO_2-ZrO_2 catalysts by XRD, Raman, and HREM techniques" J. Phys. Chem. B **109**, 3355 (2005). Additionally, grain boundaries are reported to be easier to reduce than bulk material. M. Mogensen "Ceria-based Electrodes" in Catalysis by Ceria and Related Materials , A. Trovarelli, ed., Imperial College Press, London (2002).

51. D. Duprez and C. Descorme “Oxygen Storage/Redox Capacity and Related Phenomena on Ceria-based Catalysts” in Catalysis by Ceria and Related Materials , A. Trovarelli, ed., Imperial College Press, London (2002).

52. G.-Y. Adachi and T. Masui “Synthesis and Modification of Ceria-based Materials” in Catalysis by Ceria and Related Materials , A. Trovarelli, ed., Imperial College Press, London (2002).

53. P. Fornasiero, R. di Monte, G.R. Rao, J. Kaspar, S. Meriani, A. Trovarelli, M. Graziani “Rh-Loaded CeO_2-ZrO_2 Solid-Solutions as Highly Efficient Oxygen Exchangers: Dependence of the Reduction Behavior and the Oxygen Storage Capacity on the Structural-Properties’’ J. Catal. **151**, 168 (1995).

54. In contrast to pure ceria, temperature programmed reduction of ceria-zirconia solutions typically results in only a single peak, regardless of surface area. E. Aneggi, M. Boara, C. de Leitenburg, G. Dolcetti, A. Trovarelli “Insights into the redox properties of ceria-based oxides and their implications in catalysis” J. of Alloys and Compounds **408**, 1096 (2006).

55. Other reports suggest the maximum conductivity occurs for nominal oxide vacancy concentrations of 1-3%, regardless of the rare earth or alkaline earth dopant. M. Mogensen “Ceria-based Electrodes” in Catalysis by Ceria and Related Materials , A. Trovarelli, ed., Imperial College Press, London (2002).

56. J.B. Wang, S.-Z. Hsiao, T.-J. Huang “Study of carbon dioxide reforming of methane over Ni/yttria-doped ceria and effect of thermal treatments of support on the activity behaviors” Appl. Catal.. A **246**, 197 (2003).

57. P. Vidmar, P. Fornasiero, J. Kaspar, G. Gubitosa, M. Graziani “Effects of Trivalent Dopants on the Redox Properties of $Ce_{0.6}Zr_{0.4}O_2$Mixed Oxide” J. Catal. **171**. 160 (1997).

58. G. Colon, M. Pijolat, F. Valdivieso, H. Vidal, J. Kaspar, E. Finocchio, M. Daturi, C. Binet, J.C. Lavalley, R.T. Baker, S. Bernal “Surface and structural characterization of $Ce_xZr_{1-x}O_2$ CEZIRENCAT mixed oxides as potential three-way catalyst promoters” J. Chem. Soc. Faraday Trans. **94**, 3717 (1998).

59. Z.C. Kang “Phases in the $Ce_{0.5}Zr_{0.5}O_{2-x}$ system” J. of Alloys and Compounds **408**, 1103 (2006).

60. N. Sakai, Y.O. Xiong, K. Yamaji, H. Kishimoto, T. Horita, M.E. Brito, H. Yokokawa “Transport properties of ceria-zirconia-yttria solid solutions $\{(CeO_2)_x(ZrO_2)_{1-x}\}_{1-y}(YO_{1.5})_y$ (x = 0-1, y =0.2, 0.35)” Journal of Alloys and Compounds **408**, 503 (2006).

61. E.N. Coker, M.A. Rodriguez, A. Ambrosini, R.R. Stumpf, E.B. Stechel, C. Wolverton and B. Meredig “Fundamental Materials Issues for Thermochemical H_2O and CO_2 Splitting” SAND2008-7655, December 2008.

62. See for example J.E. Funk and R.M. Reinstrom “Energy requirements in the production of hydrogen from water” Ind. Eng. Chem. Process Des. and Develop. 5 (1966) 336 and B.A. Abraham and F. Schreiner “General principles underlying chemical cycles which thermally decompose water into the elements” Ind. Eng. Chem. Fundam. 13 (1974) 305.

63. Richard Smalley “Nanotechnology and Our Energy Challenge” in Nanotechnology: Science, Innovation, and Opportunity, Lynn E. Foster, ed., Prentice Hall PTR, 2005.

64. Richard E. Smalley “Future Global Energy Prosperity: The Terawatt Challenge” MRS Bulletin 30(6) 412.

DISTRIBUTION:

10	MS 1349	James Miller, 1815
1	MS 1349	Bill Hammetter, 1815
1	MS 0887	Justine Johannes 1810
1	MS 0887	Duane Dimos, 1800
1	MS 0721	Steve Roehrig, 6300
1	MS 1104	Margie Tatro, 6200
1	MS 1104	Rush Robinett, 6330
1	MS 1110	Jeff Nelson, 6330
1	MS 0734	Ellen Stechel, 6338
1	MS 1349	Lindsey Evans, 1815
1	MS 1349	Eric Coker, 1815
1	MS 0734	Andrea Ambrosini, 6338
1	MS 1127	Rich Diver, 6335
1	MS 1127	Nathan Siegel, 6337
1	MS 0406	Fred Gelbard, 5713
1	MS 9291	Mark Allendorf, 8624
1	MS 9291	Tony McDaniel, 8367
1	MS 9409	Daniel Dedrick, 8365
1	MS 0734	Chad Staiger, 6338
1	MS 0836	Ken Chen, 1516
1	MS 0836	Roy Hogan, 1514
1	MS 1415	Gary Kellogg, 1114
1	MS 1415	Ivan Ermanoski, 114
1	MS 0123	LDRD, Donna Chavez, 1011
1	MS 0899	Technical Library, 9536 (electronic copy)


Sandia National Laboratories